Mechanical Systems and Signal Processing 160 (2021) 107830

Contents lists available at ScienceDirect

Mechanical Systems and Signal Processing

journal homepage: www.elsevier.com/locate/ymssp

Advanced optimal sensor placement for Kalman-based multiple-input estimation

R. Cumbo [a,b,*], L. Mazzanti [a,b,c], T. Tamarozzi [a,b], P. Jiranek [a], W. Desmet [b,d], F. Naets [b,d]

[a] Siemens Digital Industries Software, Interleuvenlaan 68 3001, Leuven, Belgium
[b] KU Leuven, Department of Mechanical Engineering, Celestijnenlaan 300 B, 3001 Heverlee, Belgium
[c] University of Ferrara, Engineering Department, Via Ariosto 35, 44121 Ferrara, Italy
[d] DMMS core lab, Flanders Make, Belgium

ARTICLE INFO

Article history:
Received 26 June 2020
Received in revised form 28 February 2021
Accepted 4 March 2021

Keywords:
Augmented Kalman Filter
Inverse load identification
Optimal Sensor Placement
Steady-state error covariance
Estimator bandwidth
Observability

ABSTRACT

The direct measurement of the external loads acting on a mechanical component represents often a challenge in many engineering applications. In this context, the attention of many researchers is focused on the field of inverse load identification. Several techniques are proposed in literature to address this problem by means of experimental methodologies, often coupled with simulation solutions. In this paper, a Kalman-based methodology is considered, which solves the problem of inverse load identification in a predictive manner. The common issue of most of the techniques is the selection of an optimal set of sensors which gives the best load estimation. In the Kalman-filtering framework, an Optimal Sensor Placement (OSP) strategy has been proposed by the authors and it aims to find the best set of sensors in terms of system observability, which is the minimum requirement of a stable estimation. However, this does not guarantee the most accurate load estimation. In this contribution, two alternative metrics are proposed, based on: i) steady-state error covariance of the estimation, ii) estimator bandwidth, with respect to the available set of measurements. Both criteria will be included in the existing OSP to improve the sensors selection. A comparison of the three strategies for multiple input/state estimation is discussed on an industrial-scale Finite Element Model, in order to show the improvement in the accuracy of the estimated quantities.

1. Introduction

The problem of inverse load identification is an active research topic in the field of structural mechanics since several years [1–5]. In mechanical, aerospace or civil applications, indirect load identification is of great importance in many in-service situations when the installation of transducers in the load path is intrusive or too expensive, and the load measurement cannot be obtained directly. In such cases, one interesting possibility is to identify the loads from a set of easy-to-measure responses combined with a numerical model. This is exactly the opposite framework of a forward problem, which evaluates the outputs from given inputs. The solution of the inverse load identification problem can be achieved in time or frequency domain [5], using test-based [6] or simulation-based [7–10] techniques. In this paper, the attention is focused on time-domain identification within the framework of estimators. Currently, the most widespread and used estimation algo-

* Corresponding author.
E-mail address: roberta.cumbo@siemens.com (R. Cumbo).

https://doi.org/10.1016/j.ymssp.2021.107830
0888-3270/

rithms are based on the Kalman Filtering (KF) [11,12], which can act as an optimal estimator [13]: for linear systems under the assumption of unbiased random uncertainty, the state-estimates converge to an expected value which minimizes the state covariances. The application of the KF requires the combination of both simulated and measured data. Among the broad range of Kalman filtering techniques [14–17], the Augmented Kalman Filter (AKF) [12] has recently been demonstrated to be particularly effective in the framework of load identification [17–23] on complex industrial cases. On a mechanical component, the AKF aims to identify the behavior of the system in terms of external loads (forces and torques) and full-field responses (e.g. strain, acceleration, displacement), starting from a (limited) set of response measurements (output) along the structure. Lourens et al. [17] present an application of AKF in structural dynamics, underlining the importance of using collocated or non-collocated measurements in the estimation process. Naets et al. [21] investigate the accuracy of the estimation paying attention to the stability of the filter. The presented studies proved that the type of measurements (e.g. acceleration, strain) influences the accuracy and stability of the estimation. In order to obtain a stable estimation, a number of position-level (i.e. positions, strains) outputs equal or greater to the number of forces to be identified is required. Acceleration measurements alone will lead to instability resulting from the unobservability of the system. Recent contributions [24,25] showed also the applicability of the AKF for the identification of generalized and equivalent forces.

The selection of the optimal type and location of sensors is a common issue in experimental design and inverse identification problems. Recently, Mohamed et al. [26] proposed an optimal sensor placement method for damage identification. The problem is formulated to minimize the a posteriori KF estimation error in the discrete-time formulation and it selects the optimal sensors using a recursive gradient-based screening starting from the full model. Maes et al. [27] define an optimal sensors layout for load identification by satisfying the conditions of stability and direct invertibility, which lead respectively to a minimum set of position-level and acceleration-level sensors equal to the number of forces to be estimated. The proposed approach is based on the modal characteristics of the system and it has been demonstrated in [28]. Tamarozzi et al. [29] proposed a different approach defined as Optimal Sensor Placement (OSP) strategy aimed to select the optimal type (position/acceleration/strain), number and location of the sensors needed to identify a certain set of external loads. This OSP strategy is based on three main steps [29]:

- Generation of a pool of potential sensors: random selection of limited set of sensors over the structure.
- Coarse screening: remove sensors with lower sensitivity to the input(s) to be identified.
- Observability screening: selection of sensors with highest contribution to condition number of a system observability metric.

The steps are explained in more details in [29,18]. As remarked in the last point, the focus of this method is dedicated merely to the condition number of a system observability metric. Observability is a minimum requirement to obtain a stable estimation through Kalman filtering techniques [13]. The effectiveness of this strategy for AKF estimation has been demonstrated on numerical [29] and experimental cases [20,18]. However, this approach does not allow to assess the trade-off resulting from the noise on different sensor types, and cannot take into account the impact of the sensor selection on the dynamic range of the obtained estimates.

In this work a novel Advanced Optimal Sensor Placement (AOSP) is developed and presented, which enables a more accurate a priori assessment of the impact of sensor selection. Two key metrics are proposed for the sensor selection:

- evaluation of the steady-state estimation error covariance matrix;
- evaluation of the sensor bandwidth through the transfer function between real and estimated inputs.

Within the present work, the improvement of the estimation process through the AKF is investigated in terms of used sensors. The proposed framework is numerically validated both in single and multiple input estimation cases, to illustrate the effectiveness of the filter in combination with the presented AOSP strategy. Furthermore, potential limitations of the AOSP are analyzed in details.

In Section 2, the augmented formulation of a second order structural dynamic system and the reference observability based optimal sensor placement for load identification are briefly presented. Following, the Advanced Optimal Sensor Placement is introduced and described in the two proposed formulations in Section 3. Finally, Section 4 presents a numerical validation of the proposed AOSP scheme on the input estimation of a rear twistbeam suspension, and demonstrates the superior estimation performance for sensor selected using the newly proposed AOSP scheme.

2. Problem Statement

Optimal Sensor Placement is here referred to as a selection strategy which aims to find the optimal type and location of sensors used for input-estimation through Augmented Kalman filtering techniques. In order to understand the main principle of the OSP and introduce the AOSP, the augmented state-space formulation of a dynamic system is first summarized in Section 2.1. In Section 2.2, the refernce OSP is described with main focus on the observability screening, and advantages and limitations are highlighted.

2.1. Augmented Kalman Filter for joint state-input estimation on a dynamic system

The equations of motion for a mechanical dynamic system in the continuous time-invariant first-order state-space formulation [30] are:

$$\begin{cases} \dot{\mathbf{x}}(t) = \mathbf{A}\mathbf{x}(t) + \mathbf{B}\mathbf{u}(t) \\ \mathbf{y}(t) = \mathbf{H}\mathbf{x}(t) + \mathbf{D}\mathbf{u}(t) \end{cases}, \qquad \mathbf{x} = [\mathbf{q} \quad \dot{\mathbf{q}}]^T, \tag{1}$$

where $\mathbf{x} \in \mathbb{R}^{2n_d}$, where n_d is the number of degrees-of-freedom (DoF), defines the state vector, $\mathbf{q} \in \mathbb{R}^{n_d}$ represents the generalized coordinates of the system and $\mathbf{u} \in \mathbb{R}^{n}_{i}$ (n_i = number of external loads) is the input vector. $\mathbf{A} \in \mathbb{R}^{2n_d \times 2n_d}$ and $\mathbf{B} \in \mathbb{R}^{2n_d \times n_i}$ are represented as the following real matrices:

$$\mathbf{A} = \begin{bmatrix} \mathbf{0} & \mathbf{I} \\ -\mathbf{M}^{-1}\mathbf{K} & -\mathbf{M}^{-1}\mathbf{C} \end{bmatrix}, \qquad \mathbf{B} = \begin{bmatrix} \mathbf{0} \\ \mathbf{M}^{-1}\mathbf{S_f} \end{bmatrix}, \tag{2}$$

with $\mathbf{M} \in \mathbb{R}^{n_d \times n_d}$, $\mathbf{K} \in \mathbb{R}^{n_d \times n_d}$ and $\mathbf{C} \in \mathbb{R}^{n_d \times n_d}$ as mass, stiffness and damping matrix respectively, and $\mathbf{S_f} \in \mathbb{R}^{n_d \times n_i}$ is a selection matrix of position(s) and DoF(s) related to the external load(s). The second equation of Eq. (1) defines the system measurements, where $\mathbf{y} \in \mathbb{R}^{n}_{o}$ (n_o = number of output) is the output vector, while $\mathbf{H} \in \mathbb{R}^{n_o \times n_d}$ and $\mathbf{D} \in \mathbb{R}^{n_o \times n_i}$ depend on the output response type, e.g. acceleration, position, strain [23].

In order to derive the AKF equations, the augmented state-space model is defined for the linear time-invariant system in Eq. (1), such that the unknown inputs $\mathbf{u}$ can also be considered as states. The unknown input dynamics are modelled as a random walk model due to a general lack of additional prior information on the input behavior. For the discretization of this input model we employ a zero-order hold scheme, such that the resulting augmented state model equations become:

$$\begin{cases} \dot{\mathbf{x}}^* = \mathbf{A}^* x^* \\ \mathbf{y} = \mathbf{H}^* x^* \end{cases}, \qquad \mathbf{x}^* = [\mathbf{x} \quad \mathbf{u}]^T, \qquad \mathbf{A}^* = \begin{bmatrix} \mathbf{A} & \mathbf{B} \\ \mathbf{0} & \mathbf{0} \end{bmatrix}, \qquad \mathbf{H}^* = [\mathbf{H} \quad \mathbf{D}], \tag{3}$$

where $\mathbf{x}^* \in \mathbb{R}^{(n_d+n_i)}$ and $\mathbf{A}^* \in \mathbb{R}^{n_a \times n_a}$ ($n_a = 2n_d + n_i$) are respectively the augmented state and system matrix. For a mechanical dynamic system:

- if both measurements and external inputs are known, the standard formulation of the Kalman Filter [11,12] can be applied to Eq. (1) in order to estimate the state vector.
- if the measurements are known and no information about the external input is available, the augmented formulation of the Kalman Filter [17] can be applied to Eq. (3)

From the latter statement, we can already underline that one can rely on the AKF to solve the inverse load identification only if the input location/direction is known.

The discrete-time formulation of the augmented state-space model of Eq. (3) is:

$$\begin{cases} \mathbf{x}^*_k = \mathbf{A}^*_d \mathbf{x}^*_{k-1} \\ \mathbf{y}_k = \mathbf{H}^* \mathbf{x}^*_k \end{cases}, \tag{4}$$

where $\mathbf{A}^*_d \in \mathbb{R}^{n_a \times n_a}$ is the time-discrete form of the augmented matrix $\mathbf{A}^*$ and its formulation depends on the chosen discretization scheme [31]. In the remainder of the presented theoretical analyses, we will use the continuous-time description from Eq. (3), but for the actual Kalman filter evaluation the discrete time model Eq. (4) is employed.

The observability of an inverse problem is a requirement for a stable estimation through the AKF and can be summarized as following ([32,21]):

- the number of DoFs of the structural model has to be equal or greater than the number of external loads to be estimated: $n_d \geqslant n_i$;
- the number of position/strain measurements has to be greater than the number of external loads to be estimated: $n_y \geqslant n_i$.

2.2. Optimal sensor placement strategy

An OSP strategy aims to select the optimal location, number and type of sensors needed to solve the inverse load identification through the AKF. In the frame of augmented Kalman filtering an OSP was initially developed for linear systems [29,33] and further extended for non-linear systems in [20], and this approach will serve as the reference OSP in this work. Moreover, in this contribution only linear systems are investigated. In order to perform the reference and proposed OSP, we start from two important assumptions:

- A-priori knowledge of location and direction of the loads to be identified is available;
- The minimum number of position-level sensors is equal or greater than the number of loads to be identified, which is necessary guarantee stability [21].

A scheme of the reference OSP is shown in Fig. 1 and a detailed description can be found in [29,18]. The steps grouped in the blue block are referred in this contribution to as *Training*. Once a reduced set of sensors is selected from the *coarse screening* in terms of type and location, the matrix $\mathbf{H}$ of the measurements can be defined. Each row of this matrix is scaled to have a maximum unity value. In this way, the following step (based on the Popov - Belevitch - Hautus PBH [34] criterion) will not privilege one sensor type with respect to another because of the different unit and/or different order of magnitude. The *Training* in Fig. 1 aims to bring a reduced but still sufficiently large amount of sensors to the last selecting step, i.e. *observability screening*. The latter is the key step of the reference OSP strategy and it is chosen to satisfy the stability of the AKF, which is guaranteed by the observability of the system, as stated in Section 2.1. The observability screening will be explained in details in the next subsection and investigated in terms of robustness of the strategy in Section 3.

2.2.1. Observability screening

The key idea of the reference OSP proposed in [29] is to define a combination of sensors evaluating its performance in terms of a scalar that quantifies how "observable" the system is. The observability metric used for this scope is the PBH criterion, which can be applied directly to the continuous time model or to the discrete time model as well. The two models will differ on the definition of the eigenvalues, which for one case are expected to be on the right half-plane for stable systems and in the other case in the unit circle. The stability of the system will not change from the continuous to the discrete time model if an appropriate discretization scheme is used. For the system of Eq. (3), the PBH observability matrix $\mathbf{O}_{PBH}$ is defined as:

$$\mathbf{O}_{PBH}(s) = \begin{bmatrix} s\mathbf{I} - \mathbf{A}^* \\ \mathbf{H}^* \end{bmatrix}, \tag{5}$$

In Eq. (5), the matrix $\mathbf{A}^*$ can be replaced with $\mathbf{A}_\mathbf{d}^*$ if the system of Eq. (4) is considered. A system is observable if the observability matrix O_{PBH} is of full column rank for all s in the complex plane. More in particular this implies that the system observability needs to be verified at each eigenfrequency of the augmented system, which includes natural frequencies of the structure as well as the eigenvalues associated to the input dynamics. A random walk model is introduced for the unknown load, since no information about the input entering the system is available:

$$\dot{\mathbf{u}}(t) = \mathbf{0} + \mathbf{w}_\mathbf{u}(t). \tag{6}$$

In Eq. (6), $\mathbf{w}_\mathbf{u}$ is a stochastic process with a covariance matrix $\mathbf{Q}_\mathbf{u} \in \mathbb{R}^{n_i \times n_i}$. The validation on the usage of a zeroth-order random walk model for inverse load identification and a detailed explanation on how to set the value of $\mathbf{Q}_\mathbf{u}$ matrix can be found in [18,20,21]. The eigenvalue associated to the input model in Eq. (6), which could lead to stability issues, is at $0Hz$.

The observability metric proposed in the last step of the reference OSP strategy does not directly use the PBH rank, as this is a numerically ambiguous metric, but the matrix condition number [37,38], which quantifies how close the matrix is to rank deficiency. The observability metric is proposed as following:

$$O_m = \frac{1}{n_i \cdot cond(\mathbf{O}_{PBH}(0))} \tag{7}$$

where n_i is the number of loads to estimate. There are two reasons why the PBH matrix is evaluated only at $0Hz$:

- The reference OSP mainly aims to identify the input loads and the corresponding problematic dynamics is at this frequency;
- For a real structural dynamic system, the normal modes are all damped and this leads to a detectable system, i.e. its unobservable modes are detectable [13], which is sufficient if the user is interested in input identification [32].

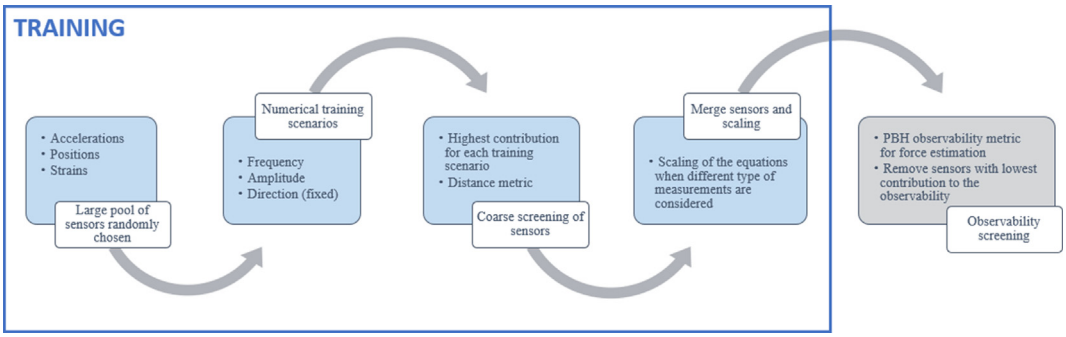

Fig. 1. Optimal Sensor Placement strategy.

If the matrix **H** includes different type of sensors, the evaluation of Eq. (7) can lead to the criterion privileging one type with respect to another (e.g. accelerometers instead of strains) because of different units and order of magnitude for the different quantities. In [18,29], the scaling of each row of **H** is proposed in order to obtain a unit-less matrix and meaningfully compare the rows of **H** associated to each sensor. The optimal set of sensors is then chosen as greedy optimization algorithm [35,36]: starting from the reduced number of sensors selected after the Training, one sensor per iteration is removed from the pool if its removal implies the lowest decrease in O_m. The final selection is identified when the decrease of O_m reaches a certain threshold fixed by the user.

2.3. An example of observability screening

A simple example is proposed on a serial 10 DoFs mass-spring system, shown in Fig. 2.

Fig. 3 shows the decrease in O_m, evaluated as in Eq. (7), for a decreasing number of sensors.

Starting from a set of measurements including position sensors on all the available DoFs, the observaility screening of Section 2.2.1 is applied and sequentially removes one sensor per iteration. In Fig. 3a, the decreasing trend is different if the measurements are expressed in [m], [mm] or scaled quantities (as applied in [18,29]). This implies that, if the user defines a threshold of observability decreasing to select the minimum set of sensors, the final selection will be different depending on which unit the measurements are expressed, which is clearly not a desired behavior. Indeed, if for example a threshold of 80% is chosen, the observability metric select a different number of sensors if the model is expressed in [m] or in [mm]. In the first case, three sensors are selected while in the second case, only one sensor is chosen. The case shown in Fig. 3a is related to a mass-normalized numerical model. If another model normalization is adopted, another trend is obtained and shown in Fig. 3b. In conclusion the index expressed in Eq. 7 defines *'how much'* a system is observable depending upon the scaling of measurements and physical system, and then naturally calls into question how this scaling should be practically done. The main reason resides in the fact that the concept of observability is generally meant to be a binary trait of a system. Thus it is in principle possible to state if a system is observable or not, but quantifying a 'degree' of observability is a much more complex issue. Moreover, this reference OSP does not account for the different noise characteristics for different sensors, or model uncertainties, which often drives sensor selection in practice.

The following subsection presents several approaches which can be adopted to improve the optimal sensor placement such that a more robust framework is obtained and to circumvent the issues described here.

3. Advanced optimal sensor placement strategy

In this work we propose a novel Advanced Optimal Sensor Placement strategy (AOSP) which revolves around two key properties which are important for any, real or virtual sensor selection:

- *Expected noise levels*: evaluating a sensor set performance by solving the Riccati equation [39] for the steady-state error covariance **P** and choosing the sensors which minimize the estimation error. As stated by Kalman and Bucy in [12] and detailed described in [13], the Kalman Filter estimation is optimal in the sense that minimizes the filtering error, i.e error covariance. The minimization of the nonlinear Riccati equation allows the definition of the optimal Kalman gain and leads thus to the best estimation. Nevertheless, other parameters, e.g. set of measurements, can affect the minimization of the error covariance, as will be explained in Section 3.1,
- *Expected dynamic range*: evaluating a sensor set performance by defining the frequency-domain transfer function between the true inputs entering the state-space system and the estimated ones. The selection resides in the sensors whose corresponding transfer function is the most relevant for the estimation.

The above metrics are proposed to replace the *observability screening* in Section 2.2.1 defining two versions of the Advanced Optimal Sensor Placement (AOSP), based respectively on the Input Error Covariance (IEC) or Transfer Function (TF). As shown in Fig. 4, the novelty of the two approaches is after the *Training*, including the measurements scaling. It will be verified that the proposed approaches are not affected by scaling issues as was the case for the reference OSP. In the following sections, these two metrics will be explained in details and then included in the AOSP.

3.1. Steady-state error covariance

Recalling Eq. (3), the linear stochastic formulation of the continuous-time augmented state-space model is:

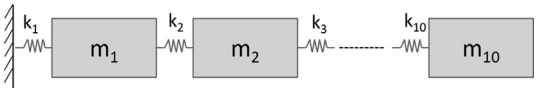

Fig. 2. 10 DoFs mass-spring system.

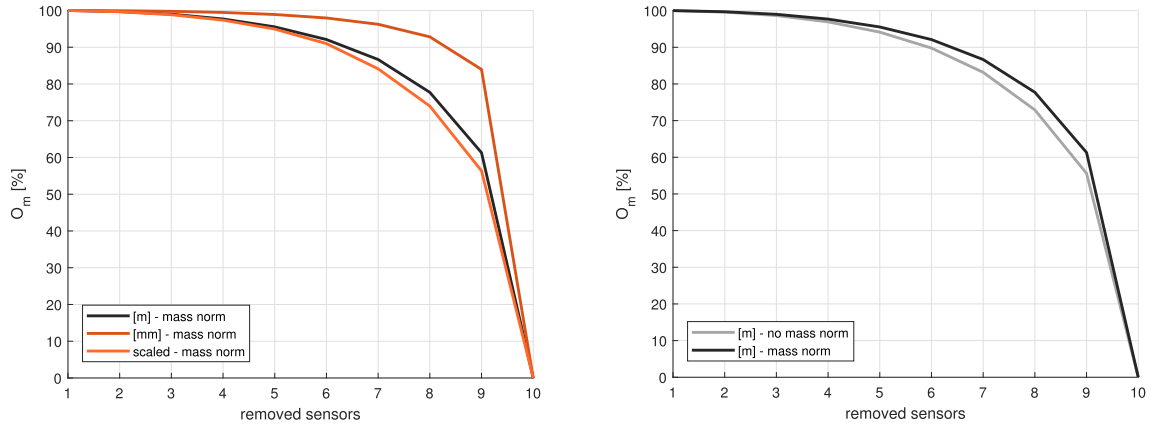

Fig. 3. Observability index decrease (percentage value of O_m indicator) obtained by the removal of position sensors through the observability screening for a 10 DoFs mass-spring system is considered.

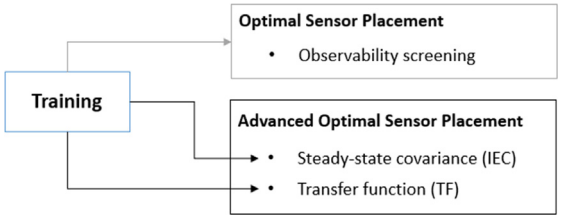

Fig. 4. Standard OSP and AOSP block scheme.

$$\begin{cases} \dot{\mathbf{x}}^* = \mathbf{A}^*\mathbf{x}^* + \mathbf{w}^* \\ \mathbf{y} = \mathbf{H}^*\mathbf{x}^* + \mathbf{v} \end{cases}, \tag{8}$$

Vectors $\mathbf{w}^*$ and $\mathbf{v}$ are mutually uncorrelated Gaussian variables (augmented process and measurement noise), with associated covariance matrices $\mathbf{Q}^* = E\{\mathbf{w}_l^*\mathbf{w}_l^{*T}\} \geqslant 0$ and $\mathbf{R} = E\{\mathbf{v}_l\mathbf{v}_l^T\} \geqslant 0$ respectively. $\mathbf{Q}^*$ is defined as a block diagonal matrix composed by $\mathbf{Q}$ and $\mathbf{Q_u}$, that are the covariance matrices referred to the model and input uncertainties respectively. Given these quantities, the filter supports the state estimation even when the precise nature of the model system is unknown [40]. An important remark is about the formulation of $\mathbf{Q}^*$: for all the studies presented in this paper, it is assumed that $\mathbf{Q} \ll \mathbf{Q}_u$, as in [18,20,21], implying that the structural model is relatively accurate with respect to the in zero-order hold input model. The main source of uncertainty therefore is $\mathbf{Q}_u$, and $\mathbf{Q}^*$ can be approximated as:

$$\mathbf{Q}^* = \begin{bmatrix} \mathbf{0} & \mathbf{0} \\ \mathbf{0} & \mathbf{Q}_u \end{bmatrix}, \tag{9}$$

$\mathbf{R}$ and $\mathbf{Q}^*$ are important parameters that characterize the AKF.

The continuous-time equivalent of the Kalman filter is also known as the Kalman-Bucy filter [12]:

$$\begin{aligned} &\dot{\hat{\mathbf{x}}}^*(t) = \mathbf{A}^*\hat{\mathbf{x}}^*(t) + \mathbf{K}_{kal}(t)(\mathbf{y}(t) - \mathbf{H}^*\hat{\mathbf{x}}^*(t)) \\ &\dot{\mathbf{P}}(t) = \mathbf{A}^*\mathbf{P}(t) + \mathbf{P}(t)\mathbf{A}^{*\mathbf{T}} + \mathbf{Q}^* - \mathbf{K}_{kal}(t)\mathbf{R}\mathbf{K}_{kal}(t)^T \\ &\mathbf{K}_{kal}(t) = \mathbf{P}(t)\mathbf{H}^T\mathbf{R}^{-1}, \end{aligned} \tag{10}$$

where $\mathbf{K}_{kal}$ represents the Kalman gain. Even though this continuous time method is not appropriate for a practical computer implementation, it is very convenient for the theoretical analysis of the estimator properties, as presented in this work. In this work, the continuous-time formulation is considered to evaluate the steady-state error covariance problem, but the discrete-time formulation could also be used. In the discrete time case, a correct selection of the discretization scheme is required to avoid inaccuracies in the covariance estimation [41], so by considering only the continuous time model in this work, we circumvent this potential issue. The second equation of Eq. (10) describes the state covariance evolution and the steady-state value, i.e. $\dot{\mathbf{P}}(t) = 0$, for a time-invariant system, leads to:

$$\mathbf{0} = \mathbf{A}^{*}\mathbf{P}(t) + \mathbf{P}(t)\mathbf{A}^{*T} + \mathbf{Q}^{*} - \left(\mathbf{P}(t)\mathbf{H}^{*T}\mathbf{R}^{-1}\right)R\left(\mathbf{P}(t)\mathbf{H}^{*T}\mathbf{R}^{-1}\right)^{T}, \tag{11}$$

which is known as the Continuous Algebraic Riccati Equation (CARE) [39,42] and its solution allows to evaluate the converged steady state error covariance for the estimators. Several approaches exist in literature to solve the CARE [43,44], and these methods are generally available in technical computing packages [45,46]. Eq. (11) allows for an optimal state estimation by means of the trace minimization of the error covariance matrix $\mathbf{P}$. The minimization defines the optimal Kalman gain $\mathbf{K}_{kal}$ [13]. With reference to the augmented state $\mathbf{x}^{*}$ in Eq. (3), the covariance matrix $\mathbf{P}$ is defined as:

$$\mathbf{P} = \begin{bmatrix} \mathbf{P}_{\mathbf{xx}} & \mathbf{P}_{\mathbf{xu}} \\ \mathbf{P}_{\mathbf{ux}} & \mathbf{P}_{\mathbf{uu}} \end{bmatrix}, \tag{12}$$

where $\mathbf{P}_{\mathbf{uu}} = E(\hat{\mathbf{u}} - \mathbf{u})(\hat{\mathbf{u}} - \mathbf{u})^{T}$ expresses the expected covariance of the unknown input error. In the case of structural dynamics, when different types of input loads are considered, e.g. forces $\mathbf{f}$ and torques $\mathbf{m}$, the augmented state $\mathbf{x}^{*}$ can be expressed as:

$$\mathbf{x}^{*} = [\mathbf{x} \quad \mathbf{u}]^{T} = [\mathbf{x} \quad \mathbf{f} \quad \mathbf{m}]^{T}, \tag{13}$$

and consequently:

$$\mathbf{P}_{\mathbf{uu}} = \begin{bmatrix} \mathbf{P}_{\mathbf{ff}} & \mathbf{P}_{\mathbf{fm}} \\ \mathbf{P}_{\mathbf{mf}} & \mathbf{P}_{\mathbf{mm}} \end{bmatrix}. \tag{14}$$

The diagonal terms of this matrix are the variances of the estimation error for each input of the systems. These are a key point in the sensor selection proposed for the IEC criterion discussed in Section 3.1.1. In the framework of an AKF, this choice resides in the direct connection between the noise obtained by a virtual sensor, i.e. estimated output, and the estimated augmented state covariance. The latter quantity also gives information about the system observability: if a system is unobservable, the solution of Eq. (11) diverges to infinity; if the system is observable, the solution of Eq. (11) converges to a finite value.

From Eq. (11), one can already observe that this metric takes into account the noise level of each measurement as well as the input uncertainty, expressed respectively by $\mathbf{R}$ and $\mathbf{Q}^{*}$, as in Eq. (9). The question that could arise from a metric based on the error covariance is if it also effectively circumvents the unit scaling issue for the measurements, as was encountered in the reference OSP shown i Section 2.3. To assess this, we consider a rescaled measurement matrix $\mathbf{H}_{\alpha}$ defined as $\mathbf{H}$ multiplied by a scaling factor α:

$$\mathbf{H}_{\alpha}^{*} = \alpha\mathbf{H}^{*}, \quad \alpha > 0 \quad . \tag{15}$$

The corresponding sensor covariance becomes:

$$\mathbf{R}_{\alpha} = \alpha^{2}\mathbf{R} \tag{16}$$

We can now substitute this rescaled sensor model in Eq. (11):

$$\begin{aligned} \mathbf{0} \quad &= \mathbf{A}^{*}\mathbf{P} + \mathbf{P}\mathbf{A}^{*\mathbf{T}} + \mathbf{Q}^{*} - \left(\mathbf{P}\mathbf{H}_{\alpha}^{*T}\mathbf{R}_{\alpha}^{-1}\right)\mathbf{R}_{\alpha}\left(\mathbf{P}\mathbf{H}_{\alpha}^{*T}\mathbf{R}_{\alpha}^{-1}\right)^{T} \\ &= \mathbf{A}^{*}\mathbf{P} + \mathbf{P}\mathbf{A}^{*\mathbf{T}} + \mathbf{Q}^{*} - \left(\mathbf{P}\alpha\mathbf{H}^{*T}\tfrac{1}{\alpha^{2}}\mathbf{R}^{-1}\right)\alpha^{2}\mathbf{R}\left(\mathbf{P}\alpha\mathbf{H}^{*T}\tfrac{1}{\alpha^{2}}\mathbf{R}^{-1}\right)^{T} \\ &= \mathbf{A}^{*}\mathbf{P} + \mathbf{P}\mathbf{A}^{*\mathbf{T}} + \mathbf{Q}^{*} - \left(\mathbf{P}\mathbf{H}^{*T}\mathbf{R}^{-1}\right)\mathbf{R}\left(\mathbf{P}\mathbf{H}^{*T}\mathbf{R}^{-1}\right)^{T} \end{aligned} \tag{17}$$

We could trivially generalize this proof to the case where α is a diagonal matrix, such that it is clear that different scalings could be applied to the different sensors. As in Eq.(17), all contributions from α cancel out, the steady-state value of $\mathbf{P}$ is not influenced by the measurement scaling, and therefore provides a more robust selection metric than the observability based criterion. In the following subsection, the steady-state estimator covariance is proposed as a sensor selection metric, i.e. Input Error Covariance (IEC), to replace the observability screening step proposed in the reference OSP.

3.1.1. Input Error Covariance (IEC) metric

In order to replace the observability screening of the reference OSP strategy, a performance indicator such as the one proposed in Eq. (7) has to be defined. The reduced set of sensors entered in the IEC step are the ones available after the Training, explained in Section 2.2. A greedy strategy is still adopted to sequentially select the sensors through the IEC. The general idea of the proposed scheme is to find a predefined number of sensors which lead to the minimal uncertainty on the estimated inputs $\mathbf{P}_{\mathbf{uu}}$. This should ideally enforce the optimal estimation of the Kalman Filter in its augmented formulation. Indeed, it is known that even if the Kalman gain is defined as optimal, a set of measurements which leads to a non-convergence of the solution exists. The minimization of the input error covariance can thus help in a more stable and accurate estimation since the input is jointly estimated with the system states and a non-convergent input estimation will lead to a non-convergence of the entire solution. In this sense, the input error covariance can be seen also as regularization parameter of the AKF: even if it can not be tuned a priori or during the estimation process, its value during the estimation plays an important role in the

convergence of the filter. The following steps are proposed to use the IEC metric for optimal sensor selection starting from a set of n_s^0 possible sensors:

1. Evaluation of Eq. (11) by using all the n_s^0 sensors selected in the *Training* $\mathbf{H}^{n_s^0} \in \mathbb{R}^{n_s^0 \times (n_d+n_i)}$. The resulting matrix defines the reference estimation error covariance $\mathbf{P_{uu}^0}$.
2. Greedy selection: at each iteration k, a set of sensors with corresponding measurement matrix $\mathbf{H}^{n_s^0-k} \in \mathbb{R}^{\left(n_s^0-k\right)\times(n_d+n_i)}$ will lead to a steady-state covariance $\mathbf{P}_{\mathbf{uu}}^k$. The removal of a single sensor from iteration k to $k+1$ is performed by evaluating the $\mathbf{P}_{\mathbf{uu}}^k$ for the removal of each sensor $g \in \mathbf{H}^{n_s^0-k}$, resulting in $\mathbf{P}_{\mathbf{uu}}^{k,g}$. The sensor $\bar{g}$ whose removal leads to the lowest increase of the trace of $\mathbf{P}_{\mathbf{uu}}^{k,g}$ matrix will will be excluded from the sensor set $\mathbf{H}^{n_s^0-\bar{k}} \in \mathbb{R}^{\left(n_s^0-\bar{k}\right)\times(n_d+n_i)}$ at the next iteration $\bar{k} = k+1$. The excluded sensor had the smallest contribution to the error covariance. This removal selection is outlined in Algorithm 1. The iterations continue until the selection reaches a desired number of $\bar{n}_s$ sensors predefined by the user.

The choice to predefine the number of sensors (rather than the required accuracy) is inspired by engineering practice where often the number of deployable sensors is limited by the number of channels available on the signal acquisition system.

Algorithm 1: IEC sensors selection

1. Execute the iterative process to find the $\bar{n}_s$ optimal sensors:
2. **for** $\mathbf{k = 0} : (\mathbf{n_s^0 - \bar{n}_s})$
3. given the measurement matrix $\mathbf{H}^{n_s^0-k}$ evaluate CARE of Eq. (11)
4. $\mathbf{P}_{uu}^k = care\left(H^{n_s^0-k}\right)$
5. Iterate on the subset of sensors $n_s^0 - k - 1$:
6. **for** $\mathbf{g = 1} : (\mathbf{n_s^0 - k - 1})$
7. remove sensor g from $\mathbf{H}^{n_s^0-k}$ to obtain $H^{n_s^0-k-1}$, with $g \notin (n_s^0 - k - 1)$
8. $\mathbf{P}_{uu}^{k,g} = care\left(H^{n_s^0-k-1}\right)$
9. Evaluate the sensor $\bar{g}$ which gives the lowest contribution to the covariance matrix:
10. $\bar{g} := min\left(trace\left(\mathbf{P}_{uu}^k\right) - trace\left(\mathbf{P}_{uu}^{k,g}\right)\right)$
11. remove sensor $\bar{g}$ from $\mathbf{H}^{n_s^0-k}$ to obtain $\mathbf{H}^{n_s^0-\bar{k}}$, with $\bar{k} = k+1$

Remark 1. when n_l input loads are considered, e.g. forces and torques, the diagonal terms of the covariance matrix $\mathbf{P_{uu}}$ will have different physical meaning and units. In order to ensure a consistent quantity in the evaluation of the trace matrix, each diagonal term j at each iteration k is normalized with respect to the corresponding value in the initial covariance matrix $\mathbf{P_{uu}^0}$ as following:

$$\overline{\mathbf{P}}_{\mathbf{uu,j}}^{\mathbf{k,g}} = \frac{\mathbf{P}_{\mathbf{uu,j}}^{\mathbf{k,g}}}{\mathbf{P}_{\mathbf{uu,j}}^{\mathbf{0}}}, \quad j = 1, \ldots, n_l \tag{18}$$

The non-dimensional terms are then mediated in order to obtain the following metric in order to replace the trace of the covariance:

$$\overline{P}^{k,g} = \frac{\sum_{j=1}^{n_l} \overline{\mathbf{P}}_{\mathbf{uu,j}}^{\mathbf{k,g}}}{n_l} \tag{19}$$

3.2. Input estimation bandwidth: Transfer Function (TF) between real and estimated input

This section aims to determine the transfer function between the load inputs applied to the dynamic system (quantity to be estimated) and the estimated inputs through the AKF in order to assess the expected dynamic performance of the input

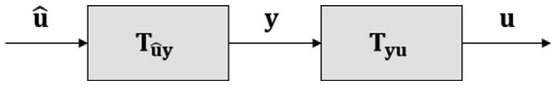

Fig. 5. Transfer function from estimated to real input loads.

estimator. The estimator is analyzed here in the Laplace domain, defining $s = i\omega = 2\pi i\phi$ (ϕ frequency content expressed in Hz). As shown in Fig. 5 the full transfer function (TF) $\mathbf{T}_{\hat{u}u}$ of the estimated and real input loads consists of two main contributions:

- $\mathbf{T}_{yu}$ real output - real input transfer function from the physical plant;
- $\mathbf{T}_{\hat{u}y}$ estimated input - real output transfer function from the AKF estimation.

It is important to remark for the following steps that the steady-state Kalman Filter [13] is considered for this analysis. This allows to work with time-invariant TFs. From past experience it has also been shown that the estimator covariance rapidly converges, such that the assumption of a steady-state filter behavior is valid [21,18]. In Fig. 6, the transfer function from Fig. 5 is shown in more detail.

The TF of the physical plant can be described as:

$$\mathbf{T_{yu}}(s) = \mathbf{HS}(s)(\mathbf{S}(s)s - \mathbf{AS}(s))^{-1}\mathbf{B} + \mathbf{D}, \tag{20}$$

such that

$$\mathbf{y}(s) = \mathbf{T_{yu}}(s)\mathbf{u}(s). \tag{21}$$

In this Eq. 20, the matrix $\mathbf{S}(s)$ is introduced and it describes the conversion of a general second order dynamic system into a first order state-space formulation in the Laplace domain. This additional transformation is necessary to account for the dynamic dependence between the displacement and velocity states which are now combined in a single state vector, as described in more detail in App. A. The matrix $\mathbf{S}(s)$ is expressed as:

$$\mathbf{S}(s) = \begin{bmatrix} \mathbf{I} & \mathbf{0} \\ \mathbf{0} & \mathbf{I}s \end{bmatrix}. \tag{22}$$

Ideally the plant transfer function would be obtained from the physical system directly. However, in practice this is not explicitly possible to determine $\mathbf{T}_{yu}$ directly. As a surrogate for the real TF, we propose to employ the same system model as employed for the Kalman filter to evaluate the TF. Even though this generally leads to an overly optimistic view on the final KF performance, it is typically the only information which is available and will allow to assess the best-case scenario for the estimator.

Next we can define the transfer function for the AKF:

$$\mathbf{T_{\hat{u}y}}(s) = \mathbf{H_u}\mathbf{S}^*(s)(\mathbf{S}^*(s)s - \mathbf{A}^*\mathbf{S}^*(s) + \mathbf{GH}^*\mathbf{S}^*(s))^{-1}\mathbf{G}, \tag{23}$$

such that

$$\hat{\mathbf{u}}(s) = \mathbf{T_{\hat{u}y}}(s)\mathbf{y}(s), \tag{24}$$

and the second order transformation matrix $\mathbf{S}^*(s)$ is (see App. A):

$$\mathbf{S}^*(s) = \begin{bmatrix} \mathbf{I} & \mathbf{0} & \mathbf{0} \\ \mathbf{0} & \mathbf{I}s & \mathbf{0} \\ \mathbf{0} & \mathbf{0} & \mathbf{I} \end{bmatrix}. \tag{25}$$

$\mathbf{G}$ is the steady-state Kalman gain matrix, which can be derived from the steady-state error covariance $\mathbf{P}^\infty$ obtained from Eq. (11), such that:

$$\mathbf{G} = \mathbf{P}^\infty(\mathbf{H}^*)^T\mathbf{R}^{-1} \quad . \tag{26}$$

Moreover, $\mathbf{H_u}$ in Eq. (23) is a boolean matrix whose purpose is the selection of the TF related to the input state included in the augmented variable $\hat{\mathbf{x}}^*$. Recalling the augmented state in Eq. (3):

$$\hat{\mathbf{u}} = \mathbf{H_u}\hat{\mathbf{x}}^* = [\mathbf{0} \quad \mathbf{0} \quad \mathbf{I}] \begin{bmatrix} \hat{\mathbf{q}} \\ \hat{\dot{\mathbf{q}}} \\ \hat{\mathbf{u}} \end{bmatrix}, \tag{27}$$

and combining the two TFs from Eq. (20) and Eq. (23), the relation between the estimated input load $\hat{\mathbf{u}}$ and the real input load $\mathbf{u}$ can be approximated (assuming the known system model):

$$\mathbf{T_{\hat{u}u}}(s) = \mathbf{T_{\hat{u}y}}(s)\mathbf{T_{yu}}(s), \qquad \hat{\mathbf{u}}(s) = \mathbf{T_{\hat{u}u}}(s)\mathbf{u}(s) \tag{28}$$

For a perfect estimator the TF should have a completely flat spectrum with gain 1, and without cross-coupling between the different inputs. However, in practice dynamic model limitations, sensor restrictions and limited tuning capabilities of the AKF scheme will inhibit this perfect behavior. In order to show that the presented TF analysis is not influenced by output

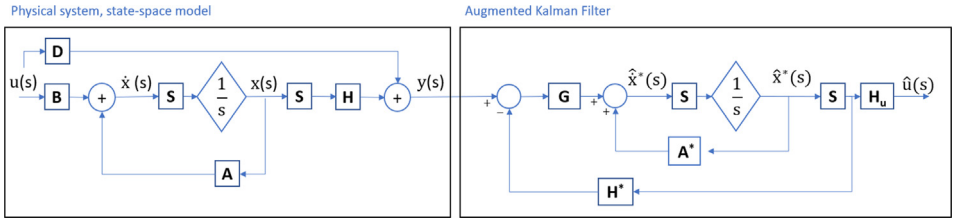

Fig. 6. Block scheme of the estimation process in Laplace domain: state-space model as input of the AKF.

scaling, the same approach proposed in Section 3.1 is adopted. Considering a scaling factor α, the following scaled matrices can be defined:

$$\mathbf{H}_\alpha = \alpha\mathbf{H}, \tag{29}$$

$$\mathbf{D}_\alpha = \alpha\mathbf{D}, \tag{30}$$

$$\mathbf{G}_\alpha = \mathbf{P}_\alpha^\infty \mathbf{H}_\alpha^T \mathbf{R}_\alpha^{-1}. \tag{31}$$

From Eq. (17) it is known that the steady-state covariance is not influenced by the scaling such that $\mathbf{P}_\alpha^\infty = \mathbf{P}^\infty$, and hence:

$$\mathbf{P}_\alpha^\infty \mathbf{H}_\alpha^T \mathbf{R}_\alpha^{-1} = \frac{1}{\alpha}\mathbf{P}\mathbf{H}^T\mathbf{R}^{-1}, \tag{32}$$

$$= \frac{1}{\alpha}\mathbf{G}. \tag{33}$$

By substituting the latter matrices in Eq. (28), it is easy to verify that the TF is not influenced by measurements scaling. Finally it is important to highlight that both $\mathbf{H}$ and $\mathbf{H}^*$ are assumed constant and frequency independent in the current analysis. This implies that the presented scheme does not account for the band-pass characteristics or internal dynamics some sensors may have. For the current work we assume that those dynamic properties are typically unknown to the developer of the estimator. However if this information is indeed available in model form, it would be possible to include this as well in the presented framework to allow for a more accurate sensor selection.

In the following subsection a metric, i.e. the Transfer Function Identity index (TFI), based on the analyzed TF is proposed to replace the observability screening of the OSP in oder to find the optimal set of sensors which gives the best input estimation in the desired frequency range. The method will be generalized for multiple-input estimation.

3.2.1. Transfer Function Identity index (TFI) metric

The target in the sensor selection is a unity value of $\mathbf{T}_{\grave{u}\grave{u}}(s)$ in the frequency range of interest, which will lead to an identity matrix for multiple-input estimation: $\mathbf{T}_{\grave{u}\grave{u}}(s) = \mathbf{I}$.

From Eq. (28) a general transfer matrix for an equal number of applied and estimated inputs can be defined as:

$$\mathbf{T}_{\grave{u}u}(s) = \begin{bmatrix} T^{11}(s) & T^{12}(s) & \dots & T^{1n_l}(s) \\ T^{21}(s) & \ddots & \vdots & \\ \vdots & & \ddots & \vdots \\ T^{n_l 1}(s) & \dots & \dots & T^{n_l n_l}(s) \end{bmatrix}, \tag{34}$$

with n_l = number of total loads to be estimated. We define the so-called identity index $I_I(s)$ to assess the similarity of the TF $\mathbf{T}_{\grave{u}u}$ to a unity matrix at a given pulsation s:

$$I_I(s) = \frac{\sum_{j=1}^{n_l} |1 - |T_{\grave{u}u}^{jj}(s)||}{n_l} + \frac{\sum_{j=1}^{n_l}\sum_{i=1,i\neq j}^{n_l} |T_{\grave{u}u}^{ji}(s)|}{n_l(n_l-1)} \tag{35}$$

The identity index $I_I(s)$ assumes a value equal to 0 when the condition $\mathbf{T}_{\grave{u}\grave{u}}(s) = \mathbf{I}$ is met. The first term of Eq. (35) expresses the average difference of the diagonal terms with respect to the target value of one. The final term introduces a penalization for the requirement on zero valued off-diagonal terms, by accounting for the average absolute value of the off-diagonal terms.

The following steps can then be defined for an optimal sensor selection:

- Definition of the frequency range of interest $\bar{\phi} = [\phi_1, \phi_2]$;

- Greedy selection strategy: at each iteration k, a set $\mathbf{H}^{n_s^0-k} \in \mathbb{R}^{\left(n_s^0-k\right)\times(n_d+n_i)}$ of sensors will give a transfer function $\mathbf{T}_{\dot{u}u}^k(\phi)$ and a corresponding identity index $I_I^k(\phi)$. The frequency spectrum of $I_I^k(\phi)$ is then averaged along ϕ in order to obtain a unique index $\bar{I}_I{}^k$. The recursive removal of one sensor from iteration k to $k+1$ is performed by evaluating the identity index for each removal of sensor $g \in \mathbf{H}^{n_s^0-k}$, resulting in $\bar{I}_I{}^{k,g}$. The sensor $\bar{g}$ whose removal gives the lowest variation of the mean index $\bar{I}_I{}^{k,g}$ will not be included in the set $\mathbf{H}^{n_s^0-\bar{k}} \in \mathbb{R}^{\left(n_s^0-\bar{k}\right)\times(n_d+n_i)}$ at the next iteration $\bar{k}=k+1$, because it means that sensor gives the lowest contribution to identity index. This removal selection is indicated in Algorithm 2. The iterations will continue until the selection of a desired number of $\bar{n}_s$ sensors fixed by the user.

Remark 2. When multiple inputs of different type, e.g. forces **F** and torques **M**, are considered in the estimation, the elements of the TF matrix in Eq. (28) are not dimensionally-consistent:

$$\hat{\mathbf{u}}(s) = \begin{bmatrix} \widehat{\mathbf{F}}(s) \\ \widehat{\mathbf{M}}(s) \end{bmatrix} = \begin{bmatrix} \mathbf{T}_{\widehat{\mathbf{FF}}}(s) & \mathbf{T}_{\widehat{\mathbf{FM}}}(s) \\ \mathbf{T}_{\widehat{\mathbf{MF}}}(s) & \mathbf{T}_{\widehat{\mathbf{MM}}}(s) \end{bmatrix} \begin{bmatrix} \mathbf{F}(s) \\ \mathbf{M}(s) \end{bmatrix} \tag{36}$$

Recalling the identity index in Eq. (35), it is possible to observe that the inconsistency is in the summation of the cross-terms of $\mathbf{T}_{\dot{u}u}(s)$. It is also true that this unit inconsistency is not meaningful for the sensors selection, since an accurate estimation should theoretically provide off-diagonal terms with negligible values. If it does not happen, the estimation accuracy is compromised, since $\mathbf{T}_{\dot{u}u} \neq \mathbf{I}$ and thus $\hat{u}_{jj} \neq u_{jj}$.

Algorithm 2: TFI sensors selection

1. Define the frequency range of interest $\bar{\phi} = [\phi_1, \phi_2]$.
2. Execute the iterative process to find the $\bar{n}_s$ optimal sensors:
3. **for** $\mathbf{k} = \mathbf{0} : \left(\mathbf{n_s^0} - \bar{\mathbf{n}}_\mathbf{s}\right)$
4. Given the measurement matrix $\mathbf{H}^{n_s^0-k}$, evaluate $\mathbf{T}_{\dot{u}u}^k$ of Eq. (28) and the identity index:
5. $I_I^k(\phi) = \frac{\sum_{j=1}^{n_I} |1-|T_{\dot{u}u}^{k,jj}(s)||}{n_I} + \frac{\sum_{j=1}^{n_I}\sum_{i=1,i\neq j}^{n_I} |T_{\dot{u}u}^{k,ji}(s)|}{n_I(n_I-1)}$
6. $\bar{I}_I{}^k = mean\left(I_I^k(\phi)\right)|_\phi$
7. Iterate on the subset of sensors $n_s^0 - k - 1$:
8. **for** $\mathbf{g} = \mathbf{1} : \left(\mathbf{n_s^0} - \mathbf{k} - \mathbf{1}\right)$
9. remove sensor g from $\mathbf{H}^{n_s^0-k}$ to obtain $\mathbf{H}^{n_s^0-k-1}$, with $g \notin \left(n_s^0 - k - 1\right)$;
10. evaluate $\mathbf{T}_{\dot{u}u}^k, g$ of Eq. (28) and the identity index $I_I^{k,g}(\phi)$;
11. $\bar{I}_I{}^{k,g} = mean\left(I_I^{k,g}(\phi)\right)|_\phi$
12. Evaluate the sensor $\bar{g}$ which gives the lowest contribution to the mean identity index:
13. $\bar{g} := min(\bar{I}_I{}^k - \bar{I}_I{}^{k,g})$
14. remove sensor $\bar{g}$ from $\mathbf{H}^{n_s^0-k}$ to obtain $\mathbf{H}^{n_s^0-\bar{k}}$, with $\bar{k} = k+1$

4. Numerical validation

In order to evaluate the effectiveness of the two metrics based on IEC and TFI in the context of input estimation, a two numerical experiments are performed and compared with the results obtained from the reference OSP. First the academic 10 mass-spring-damper system from Section 2.3 is reconsidered in Section 4.1, and next a full scale complexity structural system, modelled through a finite-element approach, is considered in Section 4.2.

4.1. Academic 10-mass-spring-damper system

The aim of this numerical example is to show the robustness of the two proposed metrics with respect to the changing of system and measurements units. In Section 2.3, a 10DoFs mass-spring-damper system has been considered in order to show the sensitivity of the PBH metric with respect to scaling issues, leading to non-consistent results. Recalling the system in Fig. 2 and considering one unknown external force acting on mass m_{10}, 10 displacement sensors are first included in the evaluation of the steady-state covariance **P** and the transfer function $\mathbf{T}_{\dot{u}u}$. The results with respect to different scale factors are shown in Fig. 7 in terms of transfer function, verifying what is stated and proof numerically in Section 3.2. The values at each frequency is constant when different scaling factors are applied. The same conclusion can be easily found for the steady-state covariance value.

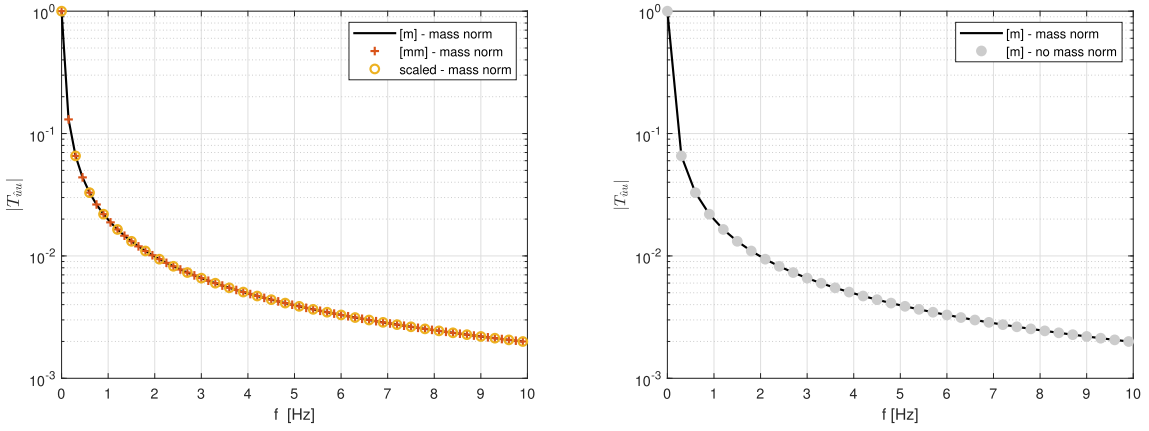

Fig. 7. Transfer function $\mathbf{T_{uu}}$ obtained by using 10 displacement sensors. On the left, comparison of the results for the mass-normalized system and i) sensors expressed in meters, ii) sensors expressed in millimiters, iii) scaled sensors. On the rigth, sensors expressed in meters and system i) mass-normalized, ii) without normalization.

In Fig. 7, a unit value of the transfer function can be observed only at 0*Hz*. By selecting an acceleration sensor on mass m_{10}, the unit value covers higher frequencies as shown in Fig. 8, which means that an improvement of the estimated input can be obtained by using a different set of sensors. A smaller value of covariance $\mathbf{P_{uu}}$ obtained with this set of sensors is shown in Fig. 9 and compared with the higher value from the set of sensors with only displacement measurements. Fig. 8 also shows the robustness of the metric with respect to scaling factors even with the usage of mixed type of sensors. The same comparison can be performed on the covariance value, which results to be insensitive to the scaling as well.

In this example, we assume to know **Q** and **R**, but a numerical experimental validation could explain the influence of both matrices. However, the investigation of this effect is out of the scope of this contribution. In the next section, a more complex system is considered for the validation of the optimal sensor selection.

4.2. Numerical validation on a Finite Element Model (FEM)

A linear FEM of a rear twistbeam suspension [47,18] shown in Fig. 10 is used for this purpose. It is defined by shell mesh with 50533 4-node quadrilateral elements. The loads are applied at the central point of the right side wheel, indicated as *input point*. The other tyre and the bushings are clamped. The target is the estimation of 6 loads, i.e. 3 forces and 3 torques, applied at the *input point* along *x*, *y* and *z* directions (reference in Fig. 10). As stated in Section 1, a minimum number of 6 position-level sensors, e.g. positions or strains, are needed to obtain a stable estimation. The target of this example is to find a set of 6 optimal strain measurements.

Four set of loads are investigated: i) sinusoidal loads with zero-phase (amplitude and frequency are listed in Table 1), ii) sweep sine loads with frequency varying from 1 Hz to 20 Hz in 5 s, iii) white noise signals, iv) impulse loads. These loads are

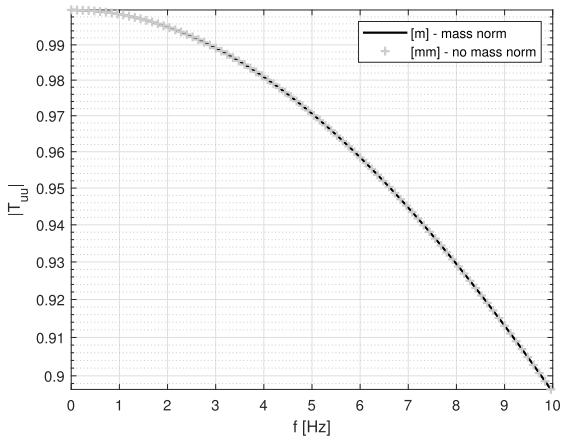

Fig. 8. Transfer function $\mathbf{T_{uu}}$ obtained by using 10 displacement sensors and 1 acceleration. Comparison of the results with sensors expressed in meters and system i) mass-normalized, ii) without normalization.

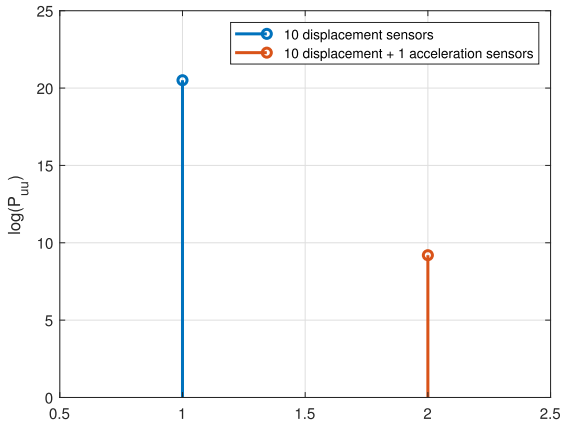

Fig. 9. Steady-state error covariance $\mathbf{P}_{\mathbf{uu}}$ value obtained by using i) 10 displacement sensors and ii) 10 displacement and 1 acceleration sensors.

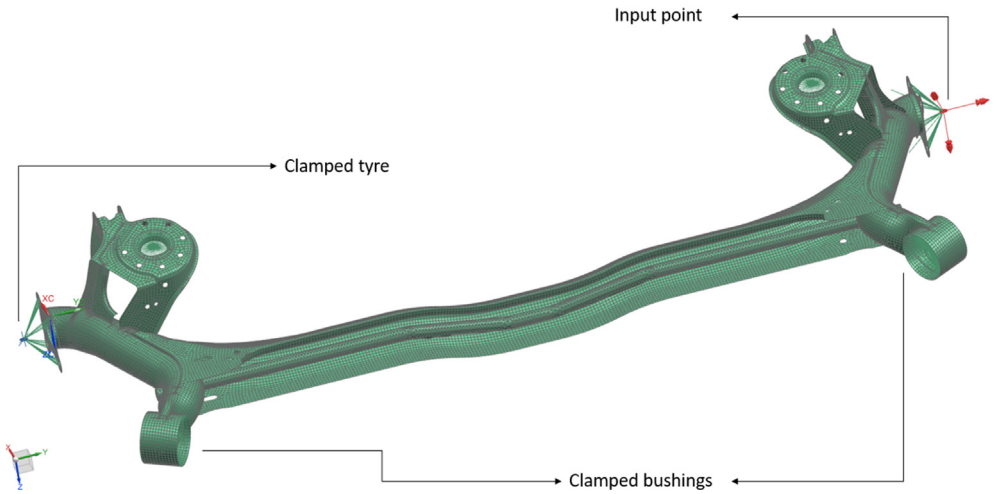

Fig. 10. FEM of the rear twistbeam suspension.

Table 1
Sine loads parameters.

Load	Amplitude	A	Frequency	ϕ
F_1	300	[N]	1	[Hz]
F_2	30	[N]	1	[Hz]
F_3	250	[N]	1	[Hz]
T_1	10000	[N mm]	1	[Hz]
T_2	65000	[N mm]	1	[Hz]
T_3	7000	[N mm]	1	[Hz]

firstly applied to execute a forward simulation and collect output responses. Gaussian noise is then added on these data and the input estimation is performed considering the loads as unknowns. Loads at low frequency are presented, but same considerations about results can be made at other frequencies since a linear model is considered. The $\mathbf{Q}_u$ value was selected using the same approach adopted in [18]. The formula is the following:

$$\mathbf{Q}_u = (\Delta t \cdot \bar{\omega}_u \cdot \bar{a}_u)^2 \quad , \tag{37}$$

with $\bar{\omega}_u$ and $\bar{a}_u$ as indicative expected value of the frequency and the amplitude of the input shape, chosen by the user.

As described in Section 2.2, before the final selection based upon PBH, IEC and TFI metrics, the *Training* procedure is performed. A starting pool of 2000 strain sensors is randomly placed on the component and the selection is then reduced to 87

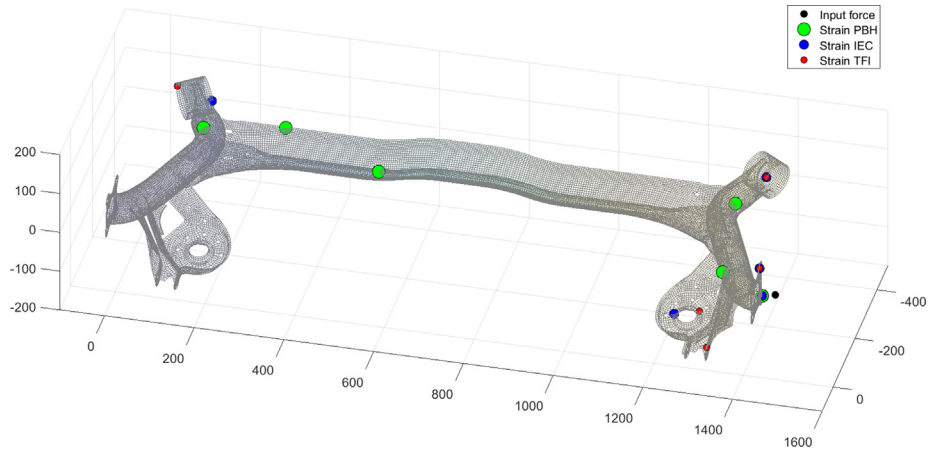

Fig. 11. Strain sensors position for the 3 criteria. The black marker indicates the *input point*.

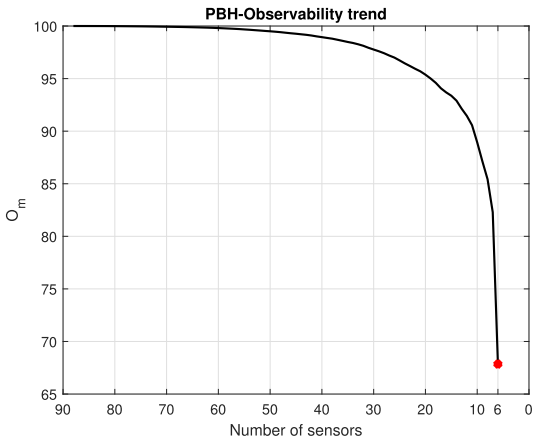

(a) O_m value in the PBH selection.

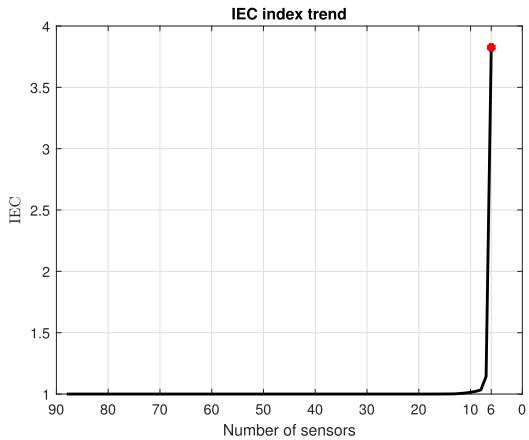

(b) $\bar{\mathbf{P}}$ value in the IEC selection.

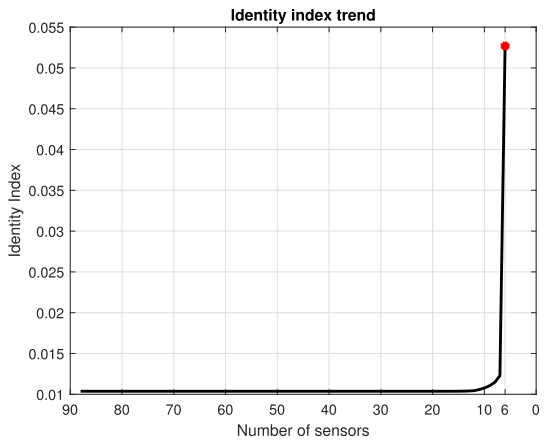

(c) I_I value in the TFI selection.

Fig. 12. Evolution of the selection indexes.

post-*Training* sensors. The selected frequency range for the TFI criteria is $[\phi_1 = 0.1, \phi_2 = 5]$ Hz, with frequency step $\Delta\phi = 0.1$ Hz. In Section 4.2.1, the results on the input estimation are shown for the two load cases and in Section 4.3 the effect of modelling errors is assessed.

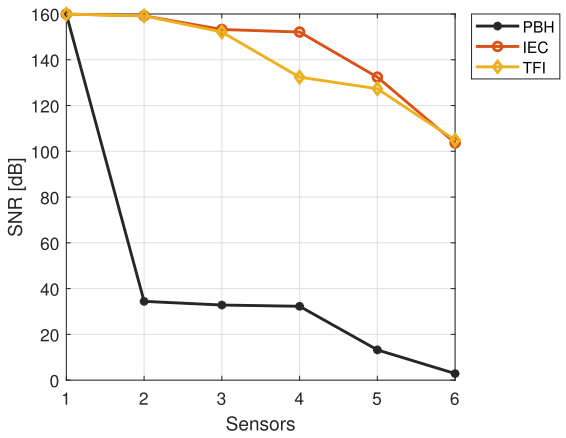

Fig. 13. SNR of the set of sensors selected by the three metrics.

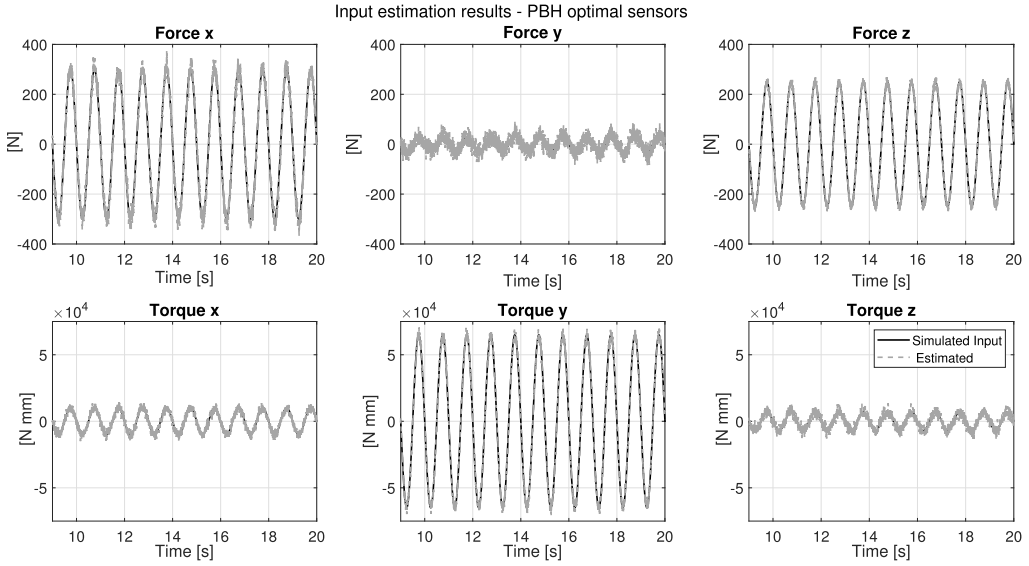

(a) Inputs estimation performed using the sensors selected by PBH criterion.

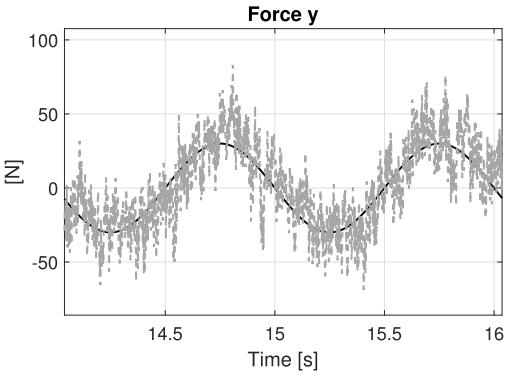

(b) Zoom of $\hat{F}_y$ shown in Fig. 14a.

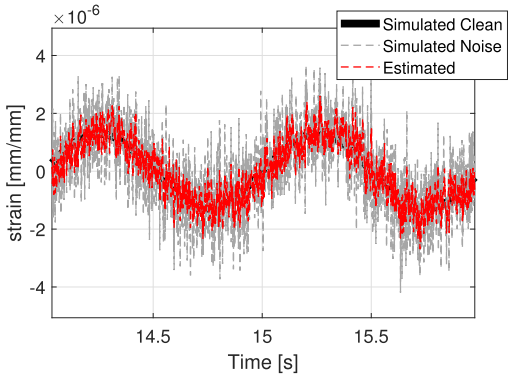

(c) One of the sensors selected by PBH criterion.

Fig. 14. .

4.2.1. Input estimation

The location of the sensors selected by PBH, IEC and TFI is shown in Fig. 11. It's possible to observe that both IEC and TFI select sensors in similar positions. It should also be noted that, since each of the starting virtual sensors represents a biaxial strain gauge, it may happen that a criteria selects one or both measurement directions for a given sensor. In Fig. 11, the PBH criterion shows 6 selected monoaxial strain sensors, while both IEC and TFI select 5 monoaxial and 1 biaxial strain sensors.

The selection indexes for the 3 criteria are shown in Fig. 12. It's possible to observe that their behavior is coherent with the effect of the removal of a sensor. O_m decreases, while $\overline{P}$ and I_I increase. The red markers in Fig. 12 indicate the value of the indexes at the last selection loop.

- *Sinusoidal loads*
  The results of the input estimation obtained using the sensors selected by the PBH criterion are shown in Fig. 14a for sine signals: the shape of the sinusoidal inputs is accurately estimated, but zooming in it's possible to observe that there's considerable noise on the estimation (Fig. 14b). The inaccuracy of the estimated signal is produced by the selection of noisy sensors. An example of sensor chosen by the PBH criterion is shown in Fig. 14c: the amount of noise on the strain signals compromises the accuracy of the estimation. In Fig. 13, the signal-to-noise ratio (SNR) of the set of sensors selected by the three metrics is compared (expressed in decibel *dB*). The SNR is evaluated as $\frac{P_s}{P_n}$, where P_s and P_n are the signal and noise power.
  This problem does not occur in the case of both IEC and TFI selection: the corresponding estimation results are shown in Fig. 15 and Fig. 16. The inputs are estimated with good accuracy and this is due to the fact that the sensors selected by both criteria have higher signal-to-noise ratio. Since both IEC and TFI consider matrix $\mathbf{R}$ and $\mathbf{Q}_u$, they are able to select the sensors that assure the most accurate output, thus leading to a lower amount of noise on the input estimation. The normalized input estimation errors are shown in Fig. 17. Each error is normalized using the difference between the real input's maximum and minimum value.
  Evaluating $I_I(\phi)$ for the selected sensors combinations at $\bar{\phi} = 1Hz$ (Fig. 18), it's possible to observe that the numerical value for the index corresponds to the accuracy of the estimations: $I_I(\bar{\phi})$ is close to 0.02 for IEC and TFI, while PBH results in $I_I(\bar{\phi}) > 0.1$. Testing the system under different conditions, it emerged that an optimal threshold value for the index is $I_I(\bar{\phi}) < 0.05$: if the selection results in an index less then this value, the inaccuracy on the estimation increases. Given these values, the performance of the set of sensors selected by IEC and TFI is due to the fact that their corresponding transfer function matrix is closer to an identity matrix if compared with the one obtained through the PBH.
- *Sine sweep loads*
  The three metrics are compared for a sine sweep signal varying from 1 Hz to 20 Hz in 5 s. The results of the sine sweep loads are shown in Fig. 19–21 and the obtained behavior is in accordance to the results obtained for the single sine load. One remark needs to be underlined for TFI estimation: the sensors have been selected in the frequency range [0.1, 5] Hz,

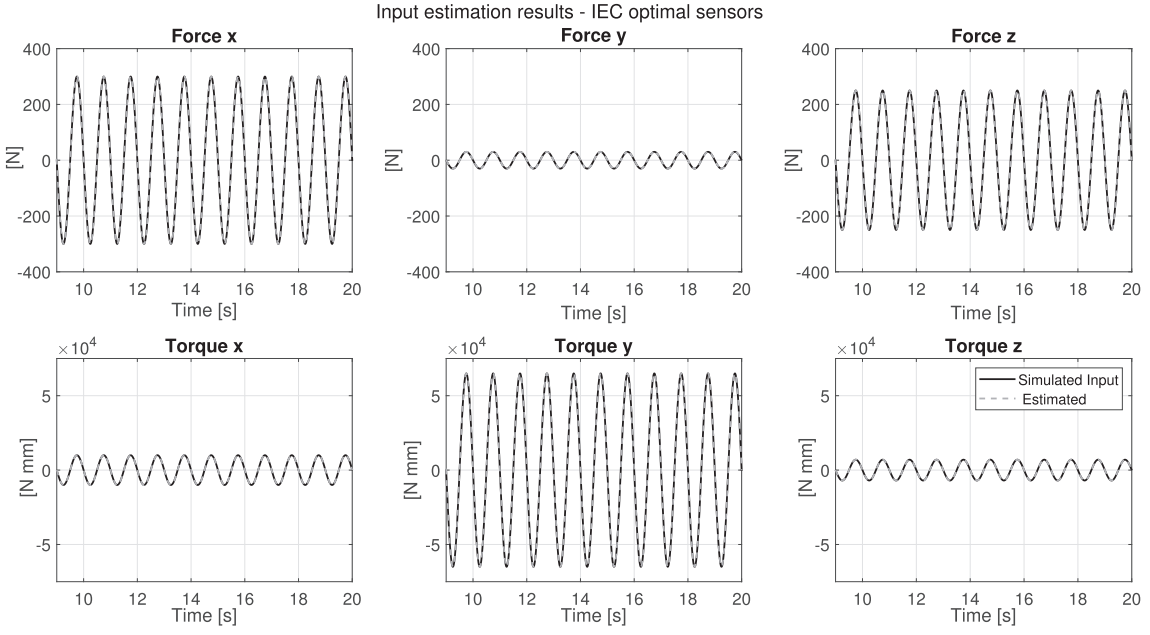

Fig. 15. Inputs estimation performed using the sensors selected by IEC criterion.

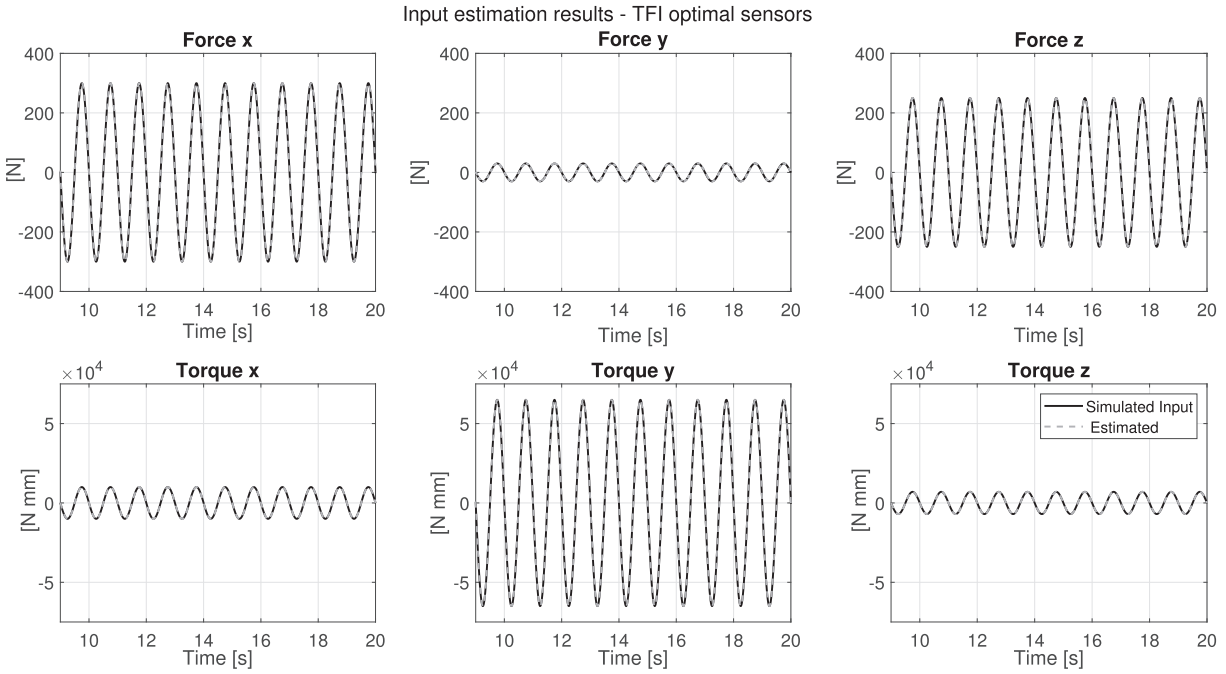

Fig. 16. Inputs estimation performed using the sensors selected by TFI criterion.

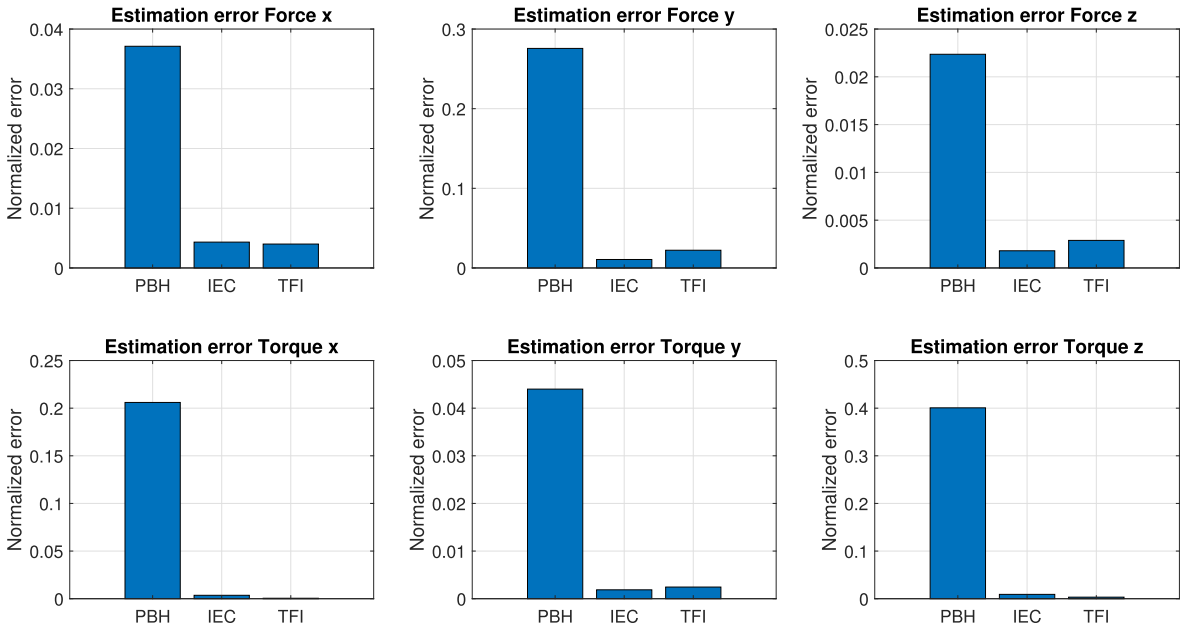

Fig. 17. Normalized error on each estimated input through sensors selected by PBH, IEC and TFI criteria.

which does not include all the frequencies excited by the input signal. More accurate results can be obtained by increasing this range. As example, Fig. 22 shows the comparison on the input load Force 2 between the estimated load for a training frequency range [0.1, 5] Hz and the one obtained by selecting the sensors in a training frequency range up to 30 Hz.

- *White noise signals*

The improvement on the input estimation can be observed on the white noise case in Fig. 23. The variance and mean value of the input signals are listed in Table 2. Fig. 23 shows the results in frequency domain f in terms of error ϵ evaluated as follows:

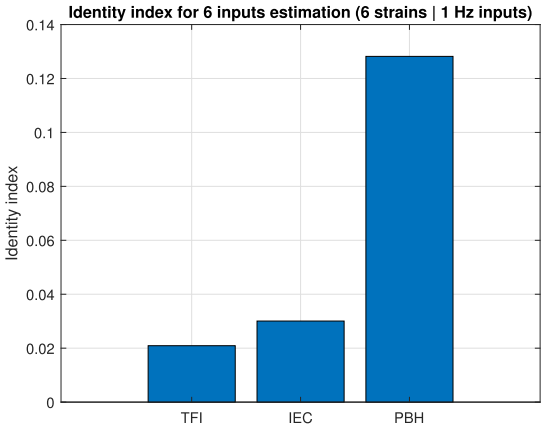

Fig. 18. Identity index evaluated at $\bar{\phi} = 1Hz$ for the 3 criteria: the numerical value reflects the accuracy of the estimations.

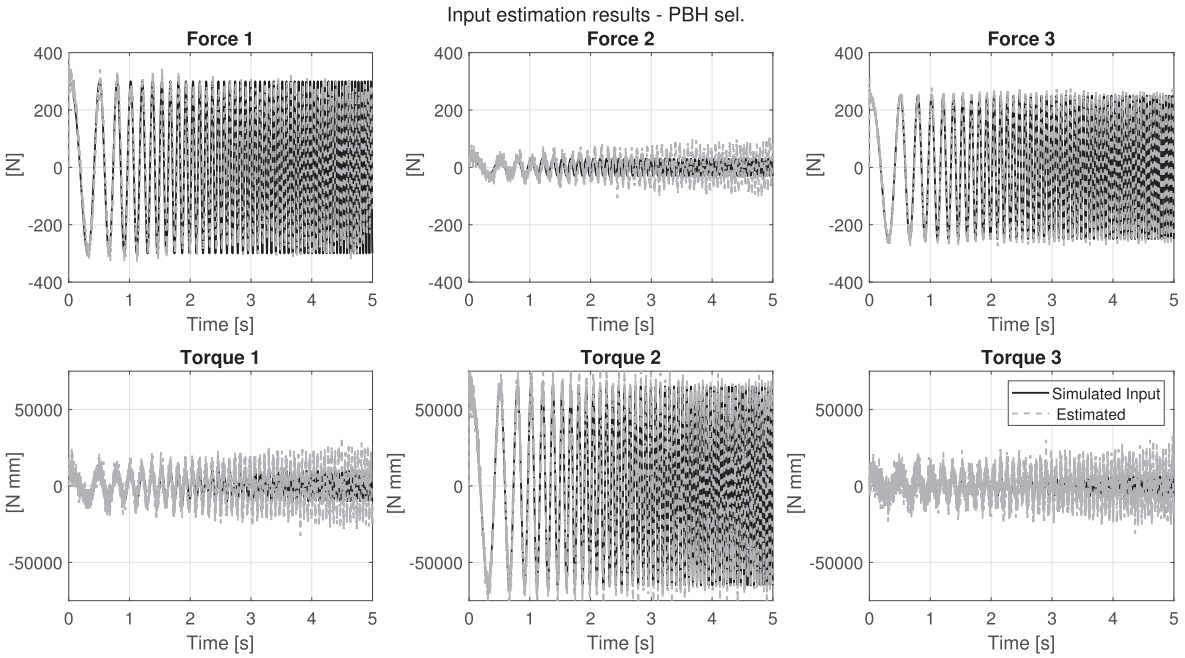

Fig. 19. Sine sweep: inputs estimation performed using the sensors selected by PBH criterion.

$$\epsilon = |log(\mathbf{u}(f)) - log(\hat{\mathbf{u}}(f))| \tag{38}$$

For illustrative purpose, Fig. 24–26 show that the overall estimation of the six loads in time domain significantly improve.

- *Impulse loads*
  For completeness of the results, the impulse loads case is considered for the estimation and the results are shown in Fig. 27–29. The conclusions on the improvement of the estimation are in line with the previous examples and thus remain unchanged.

4.3. Modelling errors

In this section, the effect of having modelling errors is investigated on the input estimation. The model used in the filter is still the same as in Section 4.2.1, thus the optimal sensor selection is not changed. The measurements used in the filter as reference data are instead generated by simulating the same model with a percentage error on the Young Modulus (E) of the material. Fig. 30 shows the evolution of the Root-Mean-Square-Error (RMSE) on forces and torques estimation obtained

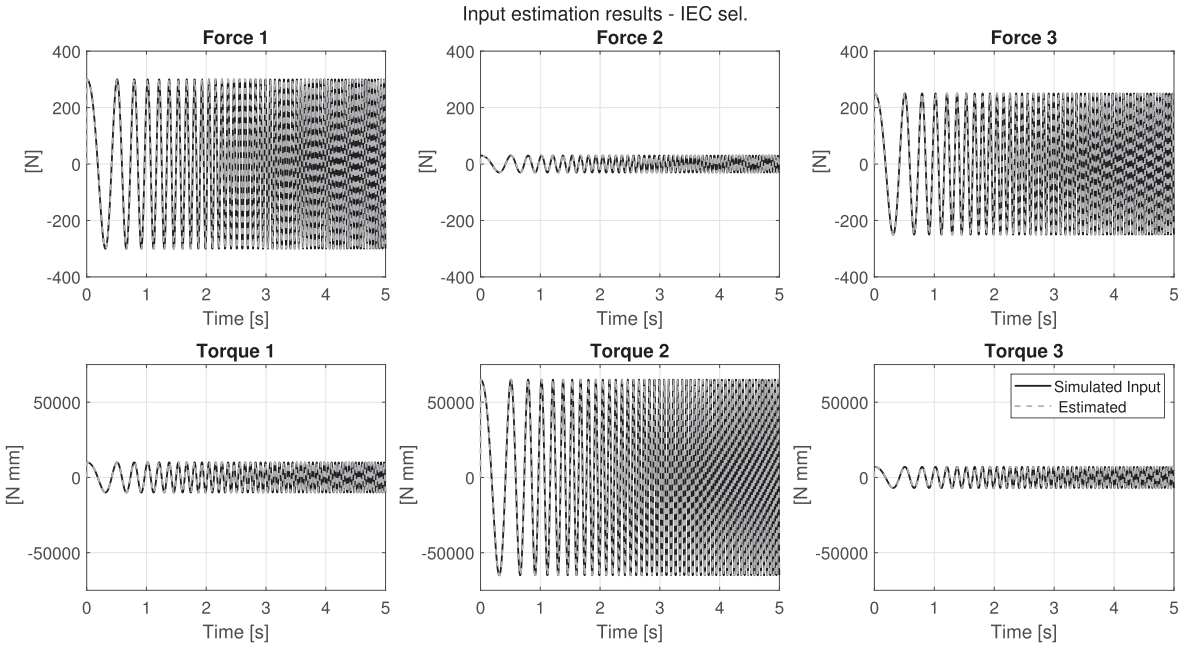

Fig. 20. Sine sweep: inputs estimation performed using the sensors selected by IEC criterion.

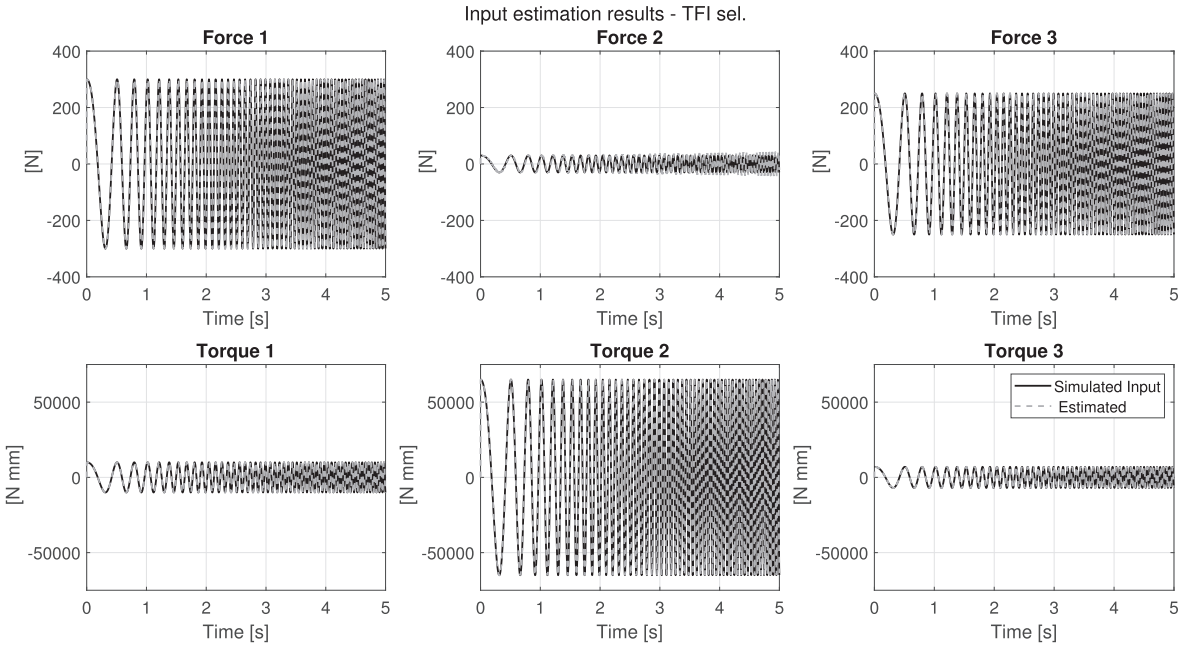

Fig. 21. Sine sweep: inputs estimation performed using the sensors selected by TFI criterion.

by increasing the percentage error of E on the set of measurements. It is possible to observe that if the modelling errors increase, the accuracy on the estimation decreases for all the metrics. This is because, as the modelling errors increase, the assumption of the input model as only source of uncertainties fails. However, the performance of the three criteria is not the same: IEC and TFI shows to be more robust to modelling errors for most of the loads.

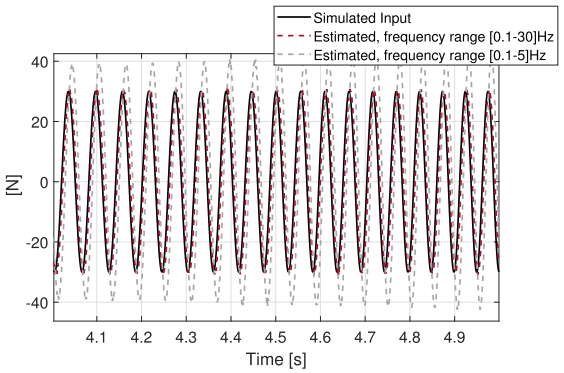

Fig. 22. Force 2 estimation performed using the sensors selected by TFI criterion in a frequency range [0.1-5]Hz and [0.1-30]Hz.

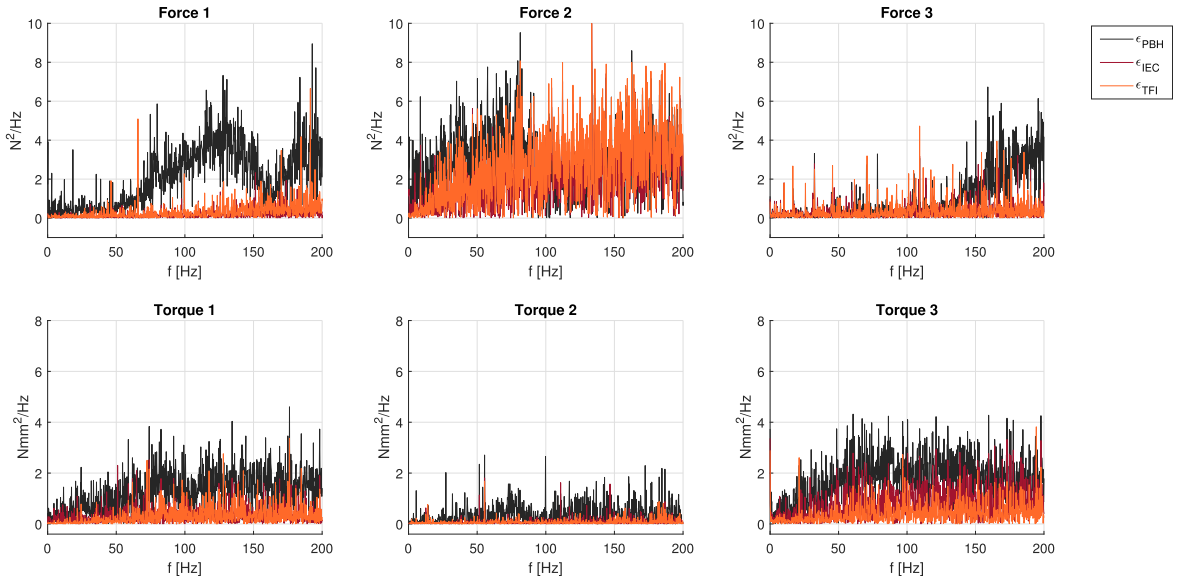

Fig. 23. White noise signal: error in frequency domain between the reference and the estimated load.

Table 2
White noise signal parameters.

Load	Variance		Mean	
F_1	9.15*E*04	[N^2]	−1.10	[N]
F_2	9.09*E*02	[N^2]	0.28	[N]
F_3	6.19*E*04	[N^2]	0.62	[N]
T_1	9.96*E*07	[N^2 mm^2]	−135.26	[N mm]
T_2	4.26*E*09	[N^2 mm^2]	1.54*E*03	[N mm]
T_3	4.92*E*07	[N^2 mm^2]	0.52	[N mm]

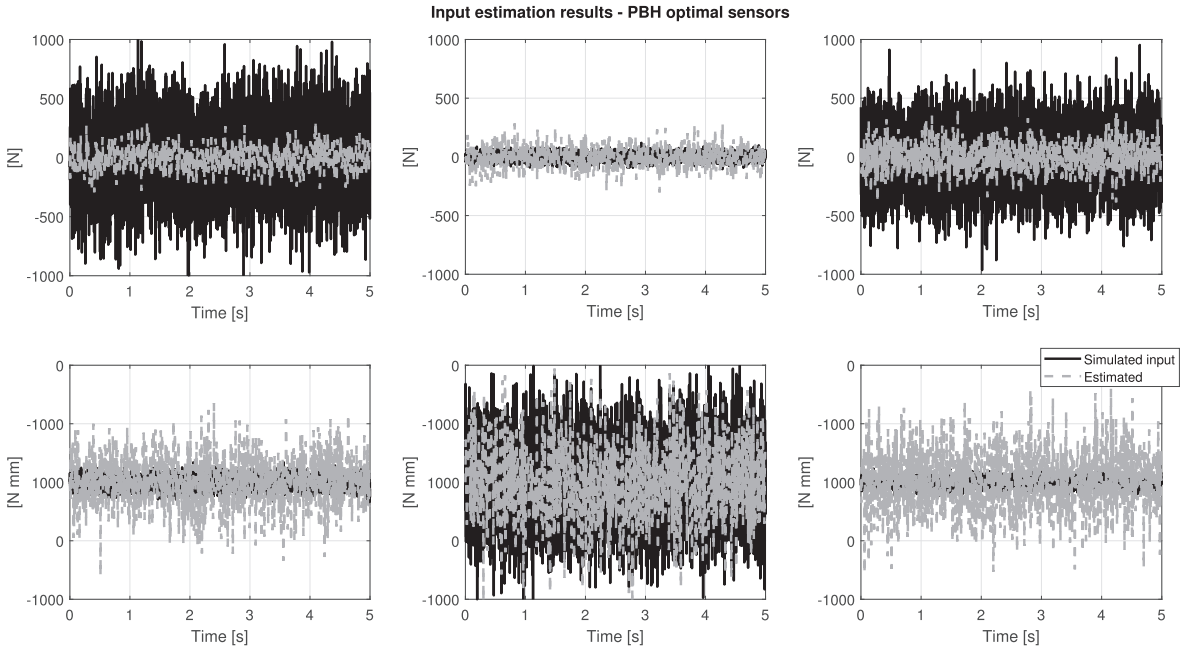

Fig. 24. White noise signal: inputs estimation performed using the sensors selected by PBH criterion.

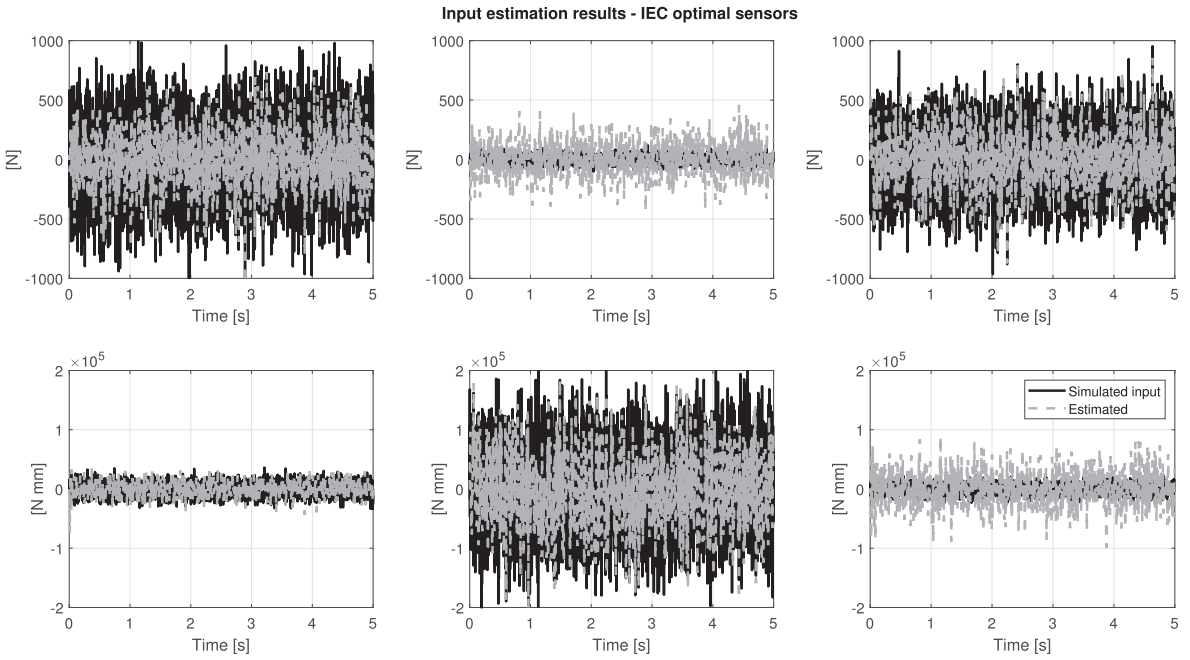

Fig. 25. White noise signal: inputs estimation performed using the sensors selected by IEC criterion.

5. Conclusions

This paper presents a novel approach for the optimal selection of sensors used for load identification of mechanical dynamic systems. An improvement on the existing Optimal Sensor Placement in the framework of AKF is proposed, replacing the observability screening criterion with more reliable approaches. Two Advanced Optimal Sensor Placement strategies are

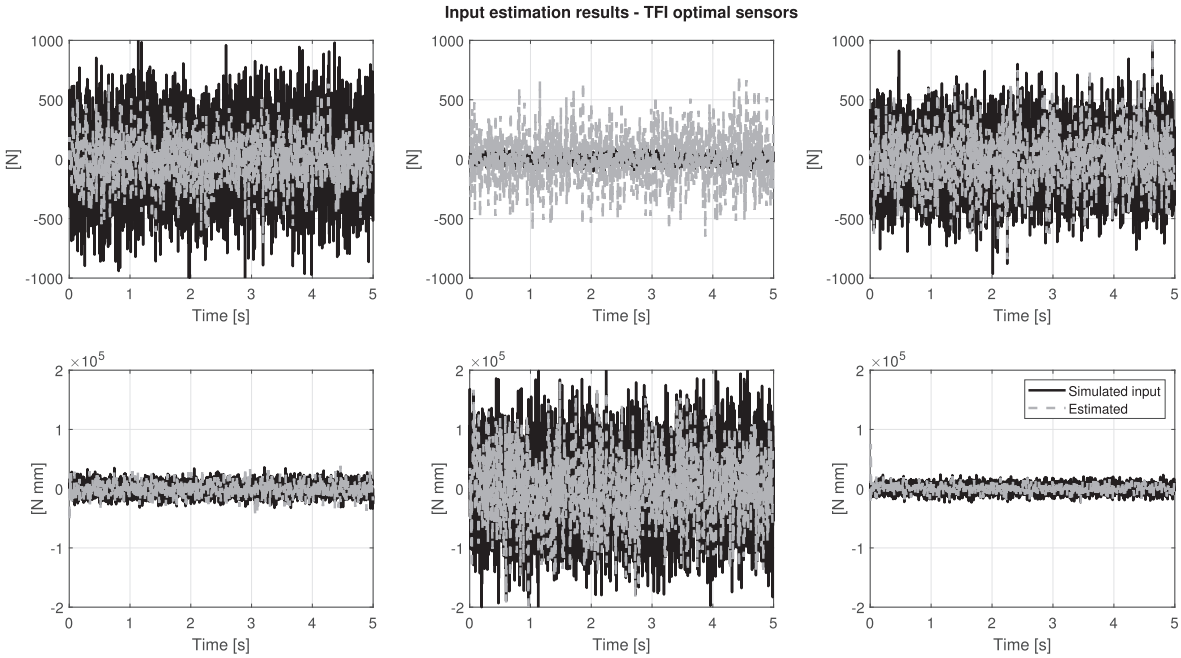

Fig. 26. White noise signal: inputs estimation performed using the sensors selected by TFI criterion.

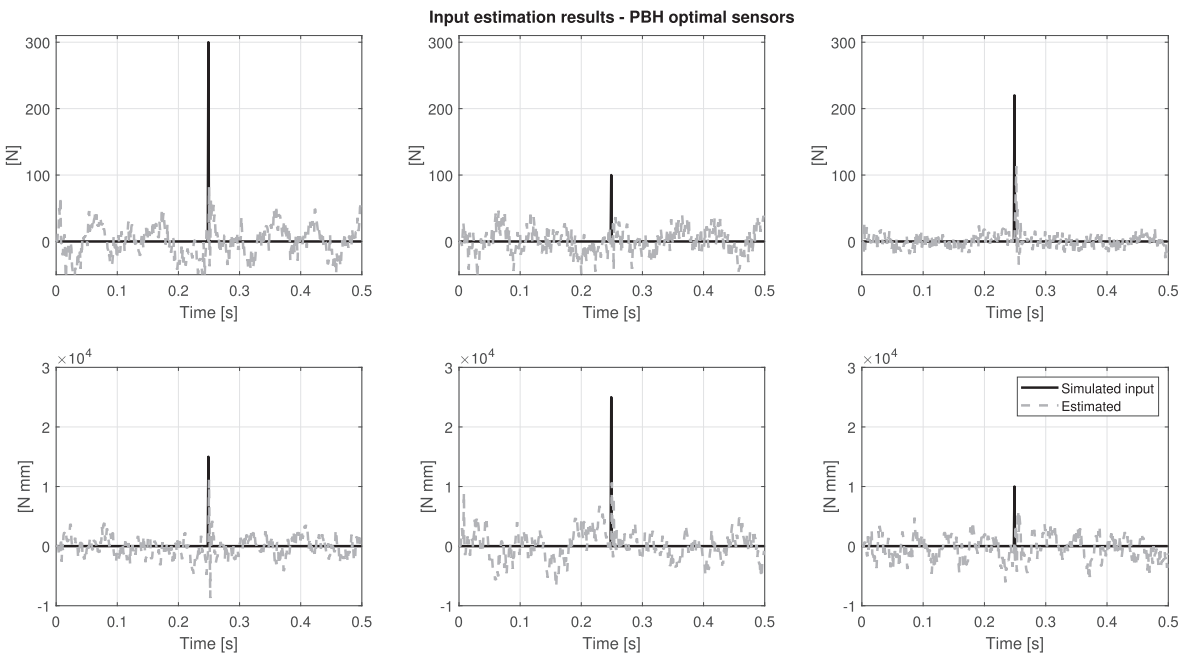

Fig. 27. Impulse loads: inputs estimation performed using the sensors selected by PBH criterion.

proposed: one based on the estimation error covariance (IEC) and the other based on the frequency domain transfer function (TFI) between the real and the estimated input. The main issue in the usage of the observability screening is in the type of sensors considered and also in the used units. The latter concerns both the units of the model itself and also the measurement equations. It is demonstrated through an example that, if position measurements expressed in [m] or [mm] are included in the selection, two different results are obtained in terms of optimal locations. Both IEC and TFI metrics are not affected by scaling problems. The effectiveness of the proposed approaches is shown through a numerical example on

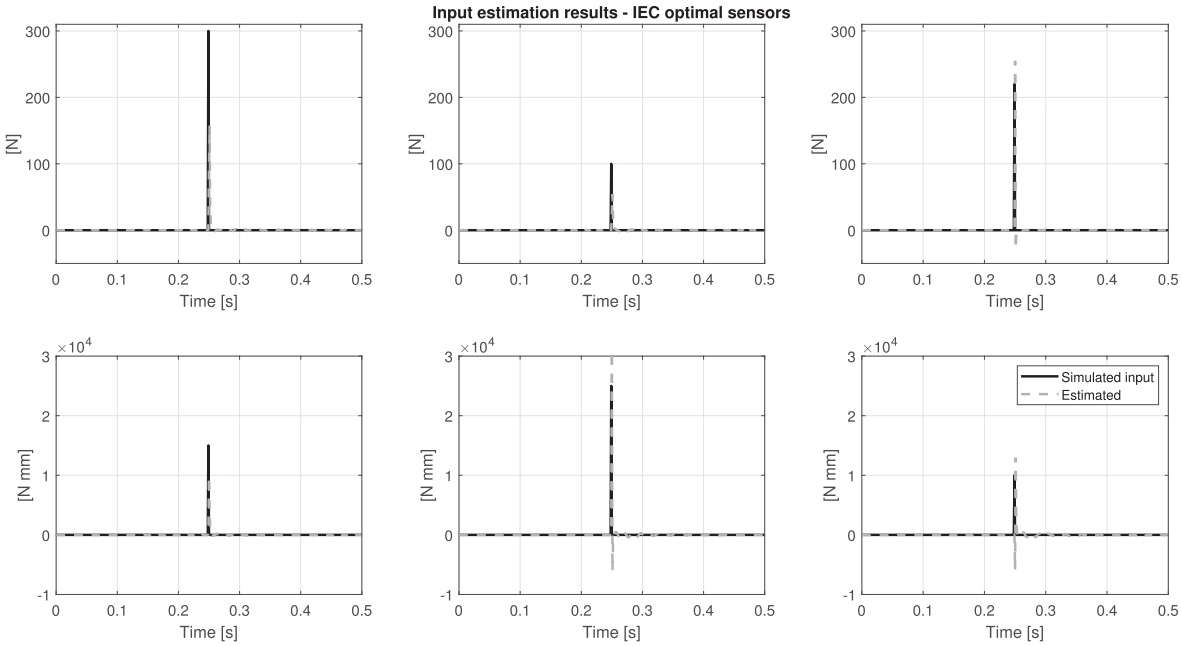

Fig. 28. Impulse loads: inputs estimation performed using the sensors selected by IEC criterion.

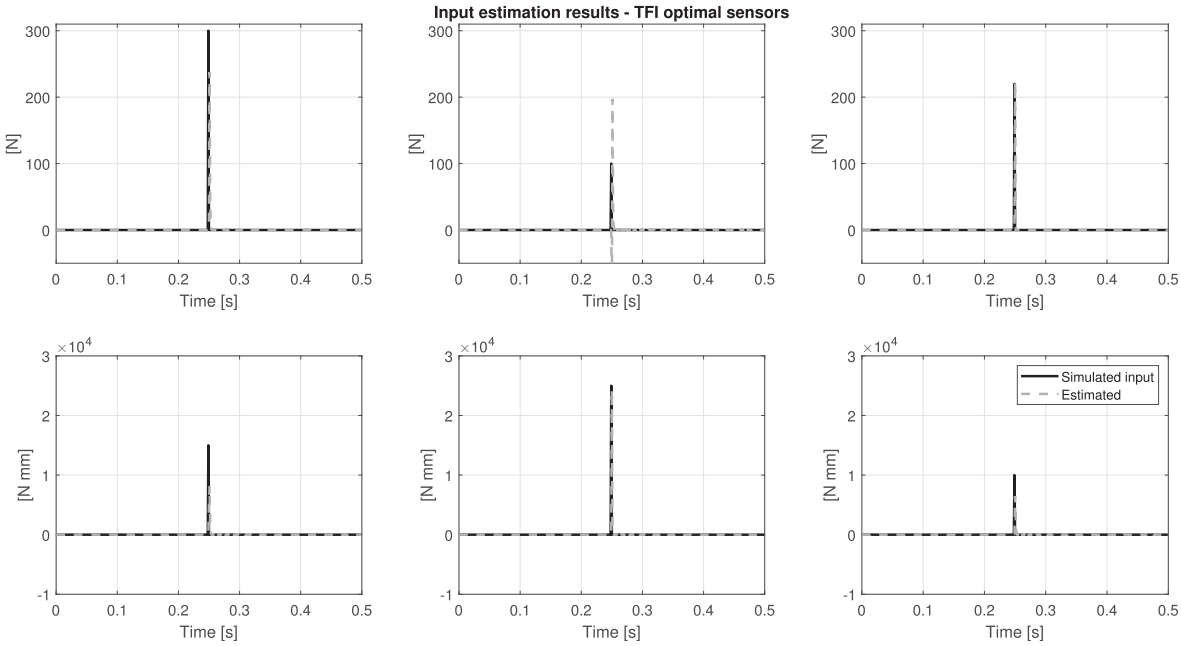

Fig. 29. Impulse loads: inputs estimation performed using the sensors selected by TFI criterion.

an industrial FE model. Multiple load estimation (3 forces and 3 torques) is performed using three different sets of sensors obtained from the two novel metrics and the existing observability screening. The results show that the estimation given by the OSP strategy is highly noisy. This can be explained underlying another issue related to this sensor selection. Indeed, it does not take into account for process and measurement covariances. The proposed approaches include intrinsically this information and it results in more accurate load estimation. Future investigation aims to test IEC and TFI metrics for multiple loads estimation on a real test case. Different load scenarios will be considered, e.g. out- and in-phase or random excitation, to evaluate the robustness of the methods.

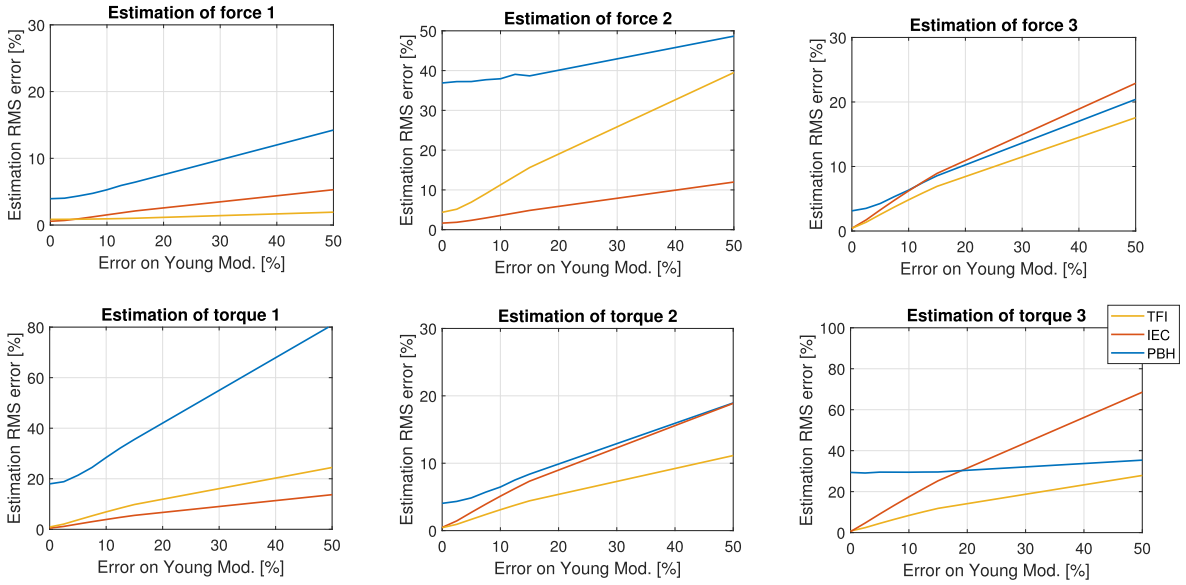

Fig. 30. RMSE value of the estimated loads for different modelling errors.

CRediT authorship contribution statement

R. Cumbo: Methodology, Supervision. **L. Mazzanti:** Data curation, Methodology, Investigation. **T. Tamarozzi:** Supervision, Conceptualization. **P. Jiranek:** Resources. **W. Desmet:** Supervision. **F. Naets:** Supervision, Methodology, Conceptualization.

Declaration of Competing Interest

The authors declare that they have no known competing financial interests or personal relationships that could have appeared to influence the work reported in this paper.

Acknowledgement

The authors gratefully acknowledge the support and contribution of VLAIO Flemish Innovation & Entrepreneurship through the Baekeland Mandate project SINCRO n. HBC.2018.2086, Flanders Make through ICON project VSFlex n. HBC.2019.0082, and the European Commission with Marie Sklodowska Curie program through the ETN ECO DRIVE project n. GA 858018.

Appendix A. Laplace transform for second order system expressed as first order system

Starting from the equation of motion of a second order mechanical dynamic system:

$$\mathbf{M}\ddot{\mathbf{x}}(t) + \mathbf{C}\dot{\mathbf{x}}(t) + \mathbf{K}\mathbf{x}(t) = \mathbf{u}(t) \tag{39}$$

the first order model is:

$$\begin{bmatrix} \dot{\mathbf{x}}(t) \\ \ddot{\mathbf{x}}(t) \end{bmatrix} = \begin{bmatrix} \mathbf{0} & \mathbf{I} \\ -\mathbf{K}/\mathbf{M} & -\mathbf{C}/\mathbf{M} \end{bmatrix} \begin{bmatrix} \mathbf{x}(t) \\ \dot{\mathbf{x}}(t) \end{bmatrix} + \begin{bmatrix} \mathbf{0} \\ \mathbf{I} \end{bmatrix} \mathbf{u}(t) \tag{40}$$

Eq. (39) and (40) are both expressed in time-domain. The corresponding first order model in Laplace Domain is:

$$\begin{bmatrix} s\mathbf{x}(s) \\ s^2\mathbf{x}(s) \end{bmatrix} = \begin{bmatrix} \mathbf{0} & \mathbf{I} \\ -\mathbf{K}/\mathbf{M} & -\mathbf{C}/\mathbf{M} \end{bmatrix} \begin{bmatrix} \mathbf{x}(s) \\ s\mathbf{x}(s) \end{bmatrix} + \begin{bmatrix} \mathbf{0} \\ \mathbf{I} \end{bmatrix} \mathbf{u}(s) \tag{41}$$

from which one can derive the matrix $S(s)$:

$$\begin{bmatrix} \mathbf{I} & \mathbf{0} \\ \mathbf{0} & s\mathbf{I} \end{bmatrix} \begin{bmatrix} s\mathbf{x}(s) \\ s\mathbf{x}(s) \end{bmatrix} = \begin{bmatrix} \mathbf{0} & \mathbf{I} \\ -\mathbf{K}/\mathbf{M} & -\mathbf{C}/\mathbf{M} \end{bmatrix} \begin{bmatrix} \mathbf{I} & \mathbf{0} \\ \mathbf{0} & s\mathbf{I} \end{bmatrix} \begin{bmatrix} \mathbf{x}(s) \\ \mathbf{x}(s) \end{bmatrix} + \begin{bmatrix} \mathbf{0} \\ \mathbf{I} \end{bmatrix} \mathbf{u}(s) \tag{42}$$

Repeating the same steps for the augmented formulation, it is easy to derive also the augmented matrix $S^*(s)$.

Appendix B. Supplementary data

Supplementary data associated with this article can be found, in the online version, athttps://doi.org/10.1016/j.ymssp.2021.107830.

References

[1] Stepan S. Simonian, Inverse problems in structural dynamics–I. Theory, Int. J. Numer. Methods Eng. 17 (3) (1981) 357–365.
[2] Gary C. Hart, James TP Yao, System identification in structural dynamics, J. Eng. Mech. Division 103 (6) (1977) 1089–1104.
[3] Daniel C. Kammer, Adam D. Steltzner, Structural identification using inverse system dynamics, J. Guidance, Control, Dyn. 23 (5) (2000) 819–825.
[4] Lars JL Nordström, T. Patrik Nordberg, A critical comparison of time domain load identification methods, in: The Proceedings of the International Conference on Motion and Vibration Control 6.2, The Japan Society of Mechanical Engineers, 2002.
[5] B.J. Dobson, E. Rider. A review of the indirect calculation of excitation forces from measured structural response data. Proceedings of the Institution of Mechanical Engineers, Part C: Mechanical Engineering Science 204.2 (1990): 69–75..
[6] Maarten V. van der Seijs, Dennis de Klerk, Daniel J. Rixen, General framework for transfer path analysis: History, theory and classification of techniques, Mech. Syst. Signal Process. 68 (2016) 217–244.
[7] Steven Gillijns, Bart De Moor, System inversion with application to filtering and smoothing in the presence of unknown inputs. Submitted for publication, KULeuven (2007).
[8] Lars JL Nordström, T. Patrik Nordberg, A time delay method to solve non-collocated input estimation problems, Mech. Syst. Signal Process. 18 (6) (2004) 1469–1483.
[9] Dionisio Bernal, Alessia Ussia, Sequential deconvolution input reconstruction, Mech. Syst. Signal Process. 50 (2015) 41–55.
[10] Tadeusz Uhl, The inverse identification problem and its technical application, Arch. Appl. Mech. 77 (5) (2007) 325–337.
[11] Rudolf E. Kalman, A new approach to linear filtering and prediction problems, J. Basic Eng. 82 (1) (1960) 35–45.
[12] Rudolf E. Kalman, Richard S. Bucy, New results in linear filtering and prediction theory, J Basic Eng. 83 (1) (1960) 95–108.
[13] Dan Simon, Optimal state estimation: Kalman, H infinity, and nonlinear approaches, John Wiley & Sons, 2006.
[14] Saeed Eftekhar Azam, Eleni Chatzi, Costas Papadimitriou, A dual Kalman filter approach for state estimation via output-only acceleration measurements, Mech. Syst. Signal Process. 60 (2015) 866–886.
[15] Øyvind Wiig Petersen et al, Estimation of the full-field dynamic response of a floating bridge using Kalman-type filtering algorithms, Mech. Syst. Signal Process. 107 (2018) 12–28.
[16] R. Palanisamy et al, Experimental validation of Kalman filter-based strain estimation in structures subjected to non-zero mean input, Smart Struct. Syst. 15 (2) (2015) 489–503.
[17] E. Lourens et al, An augmented Kalman filter for force identification in structural dynamics, Mech. Syst. Signal Process. 27 (2012) 446–460.
[18] R. Cumbo et al, Kalman-based load identification and full-field estimation analysis on industrial test case, Mech. Syst. Signal Process. 117 (2019) 771–785.
[19] R. Cumbo et al, Investigation of virtual sensing techniques on a rear twistbeam suspension by performing multiple-input/state estimation, Proc. ISMA (2018).
[20] Enrico Risaliti et al, Multibody model based estimation of multiple loads and strain field on a vehicle suspension system, Mech. Syst. Signal Process. 123 (2019) 1–25.
[21] Frank Naets, Javier Cuadrado, Wim Desmet, Stable force identification in structural dynamics using Kalman filtering and dummy-measurements, Mech. Syst. Signal Process. 50 (2015) 235–248.
[22] Risaliti, Enrico, et al. Virtual sensing of wheel center forces by means of a linear state estimator. International Conference on Noise and Vibration Engineering (ISMA2016), Leuven, Belgium. 2016..
[23] Risaliti, Enrico, et al. A state-input estimation approach for force identification on an automotive suspension component. Model Validation and Uncertainty Quantification, Volume 3. Springer, Cham, 2016. 359–369..
[24] K. Tatsis et al, A substructure approach for fatigue assessment on wind turbine support structures using output-only measurements, Procedia Eng. 199 (2017) 1044–1049.
[25] E. Lourens, D.J.M. Fallais, Full-field response monitoring in structural systems driven by a set of identified equivalent forces, Mech. Syst. Signal Process. 114 (2019) 106–119.
[26] Mohamed Khalil et al, Optimal Sensor Configuration for Fatigue Life Prediction in Structural Applications, ASME 2019 Dynamic Systems and Control Conference. American Society of Mechanical Engineers Digital Collection (2019).
[27] K. Maes et al, Design of sensor networks for instantaneous iversion of modally reduced order models in structural dynamics, Mech. Syst. Signal Process. 52–53 (2015) 628–644.
[28] K. Maes et al, Verification of joint input-state estimation for force identification by means of in situ measurements on a footbridge, Mech. Syst. Signal Process. 75 (2016) 245–260.
[29] Tamarozzi, Tommaso, et al. Noise, ill-conditioning and sensor placement analysis for force estimation through virtual sensing. International Conference on Noise and Vibration Engineering (ISMA2016), Leuven, Belgium. 2016.
[30] Bay, John. Fundamentals of linear state space systems. (1999)..
[31] Van Loan, F. Charles, Computing Integrals involving the matrix exponential, IEEE Trans. Autom. Control 23 (3) (1978) 395–404.
[32] Maes, Kristof. Filtering techniques for force identification and response estimation in structural dynamics. (2016)..
[33] Rottiers, Ward. Development of virtual measurements on a mechatronic drivetrain. (2015)..
[34] Bijoy K. Ghosh, Joachim Rosenthal, A generalized Popov-Belevitch-Hautus test of observability, IEEE Trans. Autom. Control 40 (1) (1995) 176–180.
[35] George L. Nemhauser, Laurence A. Wolsey, Marshall L. Fisher, An analysis of approximations for maximizing submodular set functions, Math. Programming 14 (1) (1978) 265–294.
[36] Nina PG Salau, Jorge O. Trierweiler, Argimiro R. Secchi, Observability analysis and model formulation for nonlinear state estimation, Appl. Math. Modelling 38 (23) (2014) 5407–5420.
[37] Biswa Datta, Numerical methods for linear control systems, Vol. 1, Academic Press, 2004.
[38] J.A. Wilson, S.Y. Guhe. Observability matrix condition number in design of measurement strategies. Computer Aided Chemical Engineering. Vol. 20. Elsevier, 2005. 397–402..
[39] William M. Wonham, On a matrix Riccati equation of stochastic control, SIAM J. Control 6 (4) (1968) 681–697.
[40] Welch, Greg, and Gary Bishop. An introduction to the Kalman filter. (1995): 41-95..
[41] M. Salgado, R. Middleton, and Graham C. Goodwin. Connection between continuous and discrete Riccati equations with applications to Kalman filtering. IEE Proceedings D (Control Theory and Applications). Vol. 135. No. 1. IET Digital Library, 1988..
[42] Rojas, Alejandro J. On the continuous-time algebraic Riccati equation and its closed-form solution. 49th IEEE Conference on Decision and Control (CDC). IEEE, 2010.
[43] Peter Benner, Alan J. Laub, Volker Mehrmann, A collection of benchmark examples for the numerical solution of algebraic Riccati equations I: Continuous-time case, Fak. f. Mathematik, TU Chemnitz, Zwickau, 1995.

[44] Hong-guo Xu, Lu. Lin-zhang, Properties of a quadratic matrix equation and the solution of the continuous-time algebraic Riccati equation, Linear Algebra Appl. 222 (1995) 127–145.
[45] https://mathworks.com/help/control/ref/care.html..
[46] https://docs.scipy.org/doc/scipy/reference/generated/scipy.linalg.solve_ continuous_are.html..
[47] Francesco Cosco, Frank Naets, Wim Desmet, Use of concept modelling for online input force estimation, ISMA Proc. (2014) 1639–1651.